Journal of Nanostructure in Chemistry
https://doi.org/10.1007/s40097-022-00498-x

ORIGINAL RESEARCH

# Towards efficient ciprofloxacin adsorption using magnetic hybrid nanoparticles prepared with κ-, ι-, and λ-carrageenan

**Sofia F. Soares[1] · João Nogueira[1] · Tito Trindade[1] · Ana L. Daniel-da-Silva[1]**

Received: 14 December 2021 / Accepted: 23 April 2022


## Abstract
The efficient removal of the antibiotic ciprofloxacin (CIP) from aqueous samples using magnetic nanosorbents prepared using three sulfated polysaccharides, κ-, ι- and λ-carrageenan and an alkoxysilane agent containing a reactive epoxide ring is described. The prepared nanosorbents were characterized in detail using FTIR spectroscopy, solid-state $^{29}$Si and $^{13}$C NMR spectroscopy and elemental microanalysis. The synthesis method was more effective for incorporating higher amounts of κ-carrageenan in the siliceous shells. Although being less sulfated, κ-carrageenan is cheaper than the other carrageenan tested. The CIP adsorption was a cooperative process, well described by the Dubinin–Radushkevich isotherm, with maximum adsorption capacities of 878, 969 and 865 mg/g for κ-, ι- and λ-carrageenan sorbents, respectively. Overall, the produced magnetic nanosorbents are among the best magnetic systems with high adsorptive efficiency for CIP. It is suggested that protonated CIP molecules are exchanged with ester sulfate counterions of carrageenan at the particles' surface as the main pathway for CIP adsorption. The adsorption process was exothermic and entropically favorable for the three sorbents. However, at 298 K, the adsorption was spontaneous for κ-carrageenan-based sorbents and non-spontaneous for ι- and λ-carrageenan particles. The magnetic sorbents could be reused and maintained their ability towards CIP removal up to four cycles. The removal efficiency in wastewater was enhanced with the sorbent dose.

### Graphical abstract

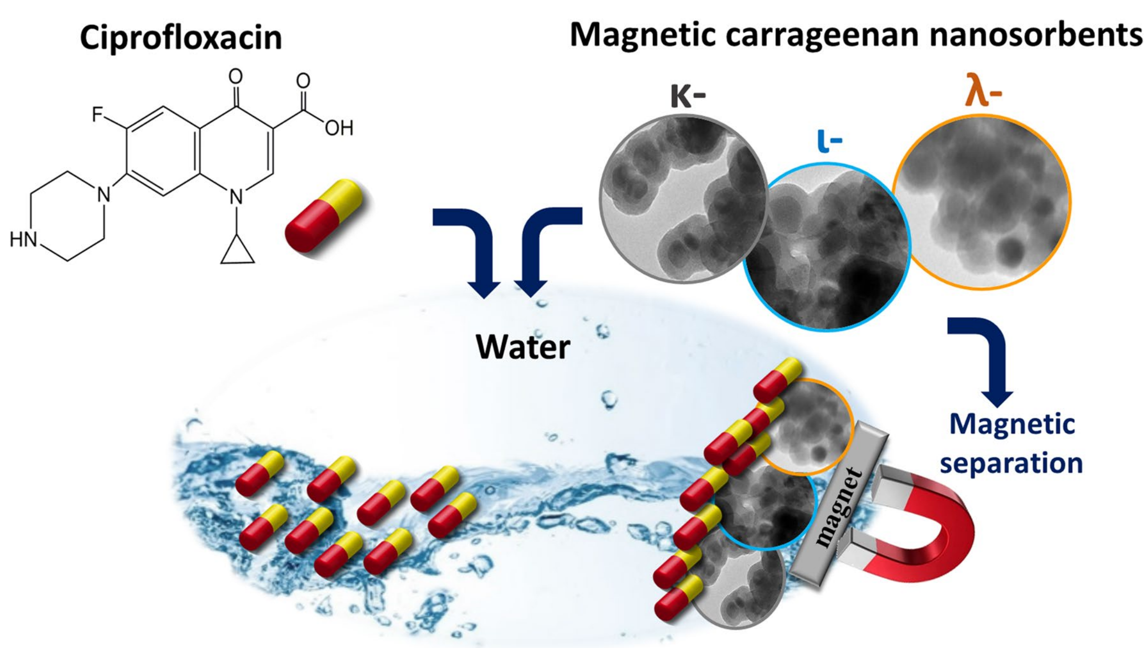


Extended author information available on the last page of the article

Published online: 19 May 2022

Magnetic carrageenan nanosorbents were prepared using three carrageenan polysaccharides (κ-, ι-, and λ-carrageenan). The resulting magnetic particles removed the antibiotic ciprofloxacin efficiently from ultra-pure water and wastewater samples. Magnetic features enabled the fast magnetic separation of the nanosorbents from water.

**Keywords** Carrageenan · Hybrids · Ciprofloxacin · Magnetite nanoparticles · Water treatment · Adsorption

## Introduction

Antibiotics in the environment are emerging pollutants that can spread antibiotic resistance, which poses a severe public health concern [1–3]. Various studies have confirmed many medicinal substances in several environmental compartments: surface waters, soil, sediment and groundwater [4–6]. Ciprofloxacin (CIP), a synthetic third-generation fluoroquinolone, is widely used as a broad-spectrum antibiotic against bacterial infections affecting humans and animals [7]. Due to their extensive use, CIP is released into the environment, likely via wastewater discharges, and is frequently detected in various aquatic environments [7, 8]. Discharges of partially treated or untreated effluents from the pharmaceutical industry, hospitals and domestic sewage are the major sources of antibiotics [9]. Several studies have reported concentrations of CIP in surface water and wastewater effluents in the ng/L–mg/L range [10, 11]. The wastewaters discharged in hospitals and pharmaceutical industries are of particular concern due to the high levels of CIP contamination, up to 150 µg/L and 31 mg/L, respectively [10, 11]. Ciprofloxacin is considered a high-risk emerging contaminant to the environment because it presents a high solubility, persistence, acute and chronic toxicity [7, 12]. The presence of CIP in wastewaters is known to cause hazardous effects on the ecosystem even at low concentrations, and therefore, its removal from wastewater is mandatory [7, 12]. Consequently, it is essential to develop sustainable methods for removing CIP from water to prevent public health risks and to mitigate the overall development of antibiotic resistance.

Nanotechnology offers many opportunities to develop nanomaterials with enhanced properties for application in various fields [13–21]. A variety of water treatment technologies have been reported for the removal of pharmaceutical compounds involving biodegradation [22], photolysis [23], membrane treatments [24], electrochemical approaches [25] and adsorption [26, 27]. Adsorption is a promising technique for water decontamination due to the affordable cost, higher performance and convenience in use [28–30]. The sorbent is a key component of the adsorption technology that determines its efficacy for a target pollutant. In an attempt to find effective sorbents, several materials have been investigated for CIP adsorption, namely activated carbon [31], carbon nanotubes [32], graphene oxide [33], aluminum [34], iron oxides [35], montmorillonite [36], kaolinite [37], birnessite [38] and polysaccharides [39, 40].

Among the polysaccharides, carrageenan has attracted attention due to its wide range of applications in the food industry, such as thickening, gelling, stabilizing agents and pharmaceutical, cosmetics, printing and textile industries [41, 42]. Carrageenan is one of the seaweed-derived biopolymers obtained by extraction from red (Rhodophyta) seaweed [42]. Carrageenans are linear sulfated polysaccharides, among which the most common are *Kappa* (κ), *Iota* (ι) and *Lambda* (λ) carrageenan. These polysaccharides differ in the sulfate substitution pattern and 3,6-anhydrogalactose content, which affects the gel-forming properties [43]. Hence, κ-carrageenan has one anionic ester sulfate group per disaccharide unit, and ι- and λ -carrageenans have two and three ester sulfate groups per disaccharide unit, respectively [42].

Apart from the conventional uses of carrageenan alone, hybrid systems of carrageenan with various natural substrates have been reported to be good candidates for the adsorption of pharmaceutical contaminants from water [39, 44–46]. Sol–gel-derived hybrid materials, where interpenetrating organic polymers and inorganic components are covalently bonded, have shown promise as sorbents [47–49]. Silicon alkoxide coupling agents have been essential in preparing such hybrid materials to enhance the compatibility between the inorganic and organic components. These coupling agents contain a specific functional group that reacts with the organic component forming strong covalent bonds, and alkoxide groups that hydrolyze and condensate to create a siliceous network [50]. Furthermore, the separation of the sorbent/pollutant system from the treated solution is a critical aspect to consider in the design of sorbents. This can be achieved using magnetic nanoparticles with functionalized surfaces that confer high affinity towards the pollutant molecules and whose magnetic features enable fast magnetic separation from the treated water [29, 51–54]. In previous works, we successfully applied this strategy to develop: (i) gelatin based magnetic bio-hybrids using epoxide and isocyanate coupling agents [50]; (ii) carrageenan and alginic acid magnetic bio-hybrids with isocyanate coupling agents for ciprofloxacin removal [39], and (iii) magnetic bio-hybrid composed of chitosan and quaternary derivatives, also modified with isocyanate coupling agents, for the adsorption of diclofenac [55].

In this work, $Fe_3O_4$ nanoparticles coated with κ-, ι- and λ-carrageenan hybrid siliceous shells were prepared, for the first time, using the epoxide functionalized 3-glycidoxypropyl trimethoxysilane (GPTMS) as a coupling agent. The chemical composition, morphology, textural and surface properties of the materials were characterized using X-ray diffraction (XRD), Fourier transform infrared spectroscopy (FTIR), scanning and transmission electron microscopy (SEM, TEM), nitrogen sorption, thermogravimetric analysis (TGA), solid-state nuclear magnetic resonance (NMR) spectroscopy and zeta potential measurements. The influencing factors of CIP adsorption by the resulting magnetic materials were studied systematically. The anionic carrageenans at the surface of the magnetic sorbents are expected to favor the adsorption of cationic species of ciprofloxacin, while the magnetic property of $Fe_3O_4$ could provide the facile separation of the particles from water. In addition, the removal of CIP in wastewater samples was investigated.

## Materials and methods

### Chemicals

Ciprofloxacin hydrochloride monohydrate ($C_{17}H_{18}FN_3O_3 \cdot HCl \cdot H_2O$, Sigma-Aldrich, 99.0%) was used in the adsorption studies. All solutions were prepared in ultra-pure water obtained from the Synergy equipment (0.22 μm filter, Milli-Q, Millipore). The polysaccharides κ-carrageenan (cat.22048, $M_w = 300{,}000$ g/mol), ι-carrageenan (cat.C1138, $M_w = 950$ g/mol) and λ-carrageenan (cat.22049, $M_w = 500{,}000$ g/mol) were acquired from Fluka BioChemica—Sigma-Aldrich and used as purchased. Regarding the preparation of magnetite nanoparticles the following chemicals were used: ferrous sulfate heptahydrate ($FeSO_4 \cdot 7H_2O$, Sigma-Aldrich, > 99%), potassium nitrate ($KNO_3$, Sigma-Aldrich, > 99%) and potassium hydroxide (KOH, LabChem, > 86%). Tetraethyl orthosilicate ($Si(OC_2H_5)_4$, TEOS, Sigma-Aldrich, > 99%) was used as a source of silica. 3-(Glycidyloxypropyl)trimethoxysilane ($C_9H_{20}O_5Si$, GPTMS, Sigma-Aldrich > 98% was used as a coupling agent. Ammonia solution (25% $NH_3$) and methanol ($CH_3OH$, > 99%) were purchased from VWR. Ethanol ($CH_3CH_2OH$, > 99%) and N,N-dimethylformamide ($HCON(CH_3)_2$, > 99%) were obtained from Carlo Erba Reagents.

### Modification of κ-, ι- and λ-carrageenan with GPTMS

Three common types of carrageenan polysaccharide (κ-, ι- and λ-carrageenan) were modified by reaction with the alkoxysilane coupling agent 3-(glycidyloxypropyl)trimethoxysilane (GPTMS). Typically, the dry carrageenan (1 g) was dispersed in dry *N*,*N*-dimethylformamide (13 mL) and GPTMS (5.2 mmol, 1.24 mL) was added. The mixture was heated to 100 °C (373 K), in nitrogen ($N_2$) atmosphere under constant stirring (500 rpm). The reaction was performed for 24 h. After cooling to room temperature, the solid was recovered and washed thoroughly with dry methanol and dry ethanol to eliminate the reaction solvent. The resulting powders were dried at room temperature. Three different derivatized polymers were obtained, hereafter designated κ-CRG/GPTMS, ι-CRG/GPTMS and λ-CRG/GPTMS.

### Synthesis of magnetic hybrid particles with κ-, ι-, and λ-carrageenan

The magnetic particles coated with hybrids of κ-, ι-, and λ-carrageenan and GPTMS were prepared in two steps. The magnetic core consisting of magnetite nanoparticles ($Fe_3O_4$) were synthesized starting from an aqueous solution of $Fe_2SO_4.7H_2O$ as previously reported [56]. Then, the coating was performed through the sol–gel method in the presence of the magnetic cores, employing a mixture of TEOS with the modified polymers κ-CRG/GPTMS, ι-CRG/GPTMS and λ-CRG/GPTMS. Typically, 40 mg of $Fe_3O_4$ nanoparticles was dispersed in 38 mL of ethanol, under sonication (horn Sonics, Vibracell) for 15 min in an ice bath. Then, 0.406 mL of TEOS and 0.3 g of the carrageenan derivative were added to the mixture, following by the addition of 2.4 mL of ammonia. The reaction was sonicated for two hours, immersed in an ice bath. The produced particles were separated magnetically from the solution using a NdFeB magnet and washed successively with ethanol. Finally, the magnetic particles were left to dry by evaporation of the solvent. Three different magnetic hybrid particle samples were obtained, $Fe_3O_4$@$SiO_2$/κ-CRG/GPTMS, $Fe_3O_4$@$SiO_2$/ι-CRG/GPTMS and $Fe_3O_4$@$SiO_2$/λ-CRG/GPTMS.

### Synthesis of non-magnetic κ-, ι-, and λ-carrageenan/silica hybrid particles

The non-magnetic hybrid particles were obtained by hydrolysis and condensation of a mixture of the modified carrageenan (κ-CRG/GPTMS, ι-CRG/GPTMS and λ-CRG/GPTMS) with TEOS in a homogeneous alcoholic medium containing water and using a base as a catalyst. Briefly, the modified carrageenan (0.3 g) and TEOS (0.406 mL) were mixed in an Erlenmeyer flask containing deionized water (0.9 mL). Then, ethanol (8.5 mL) and ammonia solution (0.15 mL) were added to the mixture, under constant stirring (250 rpm), for 24 h at room temperature. After the reaction, the materials were washed five times with deionized water and one time with ethanol, followed by centrifugation. Finally, the solvents were evaporated, and three non-magnetic hybrid particles were obtained ($SiO_2$/κ-CRG/GPTMS, $SiO_2$/ι-CRG/GPTMS and $SiO_2$/λ-CRG/GPTMS). For comparative purposes, $SiO_2$ particles have also been prepared using the Stöber method [57].

## Characterization of materials

Fourier transform infrared (FTIR) spectra with attenuated total reflectance (ATR) of the particles were collected using a spectrophotometer Bruker Tensor 27, at 4 $cm^{-1}$ of resolution and 256 scans. The X-ray powder diffraction (XRD) data were collected using a PANalytical Empyrean X-ray diffractometer equipped with the Cu Kα monochromatic radiation source at 45 kV/40 mA. The elemental analysis was performed using a Leco Truspec-Micro CHNS 630-200-200 equipment. The specific surface area was measured by $N_2$ sorption experiments at − 196 °C after sample degasification at 80 °C under nitrogen flow overnight using a Gemini V2.0 surface analyzer (Micromeritics Instrument Corp.).The specific surface area was calculated using Brunauer–Emmett–Teller (BET) isotherm and the pore volume using the Barret–Joyner–Halenda (BJH) method. Scanning electron microscopy (SEM) images were obtained using a Hitachi SU-70 microscope operating at an accelerating voltage of 15 kV. Transmission electron microscopy (TEM) analysis was done in a Hitachi H-9000 TEM microscope operated at 300 kV. The SEM samples were prepared by placing a drop of a dilute ethanolic suspension of the particles over a glass slide glued to the sample holder using double-sided carbon tape. After evaporating the sample was coated by carbon sputtering. For TEM analysis, the samples were prepared by evaporating an ethanolic suspension of the nanoparticles deposited on a copper grid coated with an amorphous carbon film. Thermogravimetric analysis (TGA) of the materials was carried out in a TGA 50 instrument from Shimadzu. The TGA measurements were performed under a nitrogen atmosphere, and the samples were heated from 25 to 900 °C at a rate of 10 °C $min^{-1}$. The $^{13}C$ CP (cross-polarization)/MAS (magic-angle spinning) NMR (nuclear magnetic resonance) and $^{29}Si$ MAS NMR spectra were recorded on a Bruker Avance III 400 MHz (9.4 T) spectrometer at 79.49 and 100.61 MHz, respectively. $^{29}Si$ MAS NMR spectra were recorded with 4.5 µs 1H 90° pulses, a recycle delay of 60 s, and at a spinning rate of 5 kHz. $^{13}C$ CP/MAS NMR spectra were recorded with 3.65 µs $^{1}H$ 90° pulses, 1.5 ms contact time, a recycle delay of 5 s, and a spinning rate of 9 kHz. Chemical shifts are quoted in ppm relative to tetramethylsilane (TMS). The surface charge of the particles was assessed by measuring the zeta potential in a Zetasizer Nano ZS equipment (Malvern Instruments).

## Adsorption experiments

The adsorptive performance of the magnetic hybrid particles was evaluated in batch adsorption experiments. Briefly, the magnetic hybrid sorbents were accurately weighed, added to glass vials with CIP solution and shaken, at 30 rpm, in an overhead shaker, at 25.0 ± 2.0 °C. Before the adsorption experiment, CIP stock solutions were prepared in ultra-pure water and shaken, at 100 rpm, overnight in dark conditions. After the corresponding shaking period, the magnetic hybrid sorbent was separated magnetically from solution using a NdFeB magnet, which was analyzed spectrophotometrically by monitoring the absorbance at 273 nm, in a Jasco U-560 UV–VIS spectrophotometer, for the residual CIP concentration. The calibration curve was performed in ultra-pure water and used to convert the absorbance into CIP concentration (Figure S1, Supporting Information).

### Effect of pH

The performance of the magnetic hybrid particles for removing CIP from ultra-pure water was studied at distinct pH values (5, 6, 7 and 8) by adjusting the solution pH with HCl (0.01 M) or NaOH (0.01 M) solutions. An initial CIP concentration of 60 mg/L and a fixed sorbent dose of 0.5 mg/mL were used. The contact time was 24 h, to ensure that the sorption equilibrium was reached. Afterwards, the magnetic hybrid particles were separated magnetically using a NdFeB magnet. The amount of CIP adsorbed at each time ($q_t$, mg/g) was determined by Eq. (1):

$$q_t = \left(C_0 - C_t\right) \times \frac{V}{m}, \tag{1}$$

where $C_0$ (mg/L) is the initial concentration of CIP, $C_t$ (mg/L) is the CIP concentration in the treated solution at time $t$, V is the volume of solution (L) and m is the sorbents mass (g).

### Kinetic adsorption studies

The CIP adsorption time profile was assessed to investigate the kinetics of adsorption. Solutions of CIP were prepared (100 and 200 mg/L) by diluting the stock CIP solution in ultra-pure water, and the batch experiments were conducted at an initial pH of 5. The sorbent dose tested was 0.5 mg/mL in all the kinetic experiments. Then, the system was shaken during 3 h (180 min) under controlled room temperature (25.0 ± 2.0 °C), and aliquots were collected along the time. After analysis of the supernatant in a UV–VIS spectrophotometer, the amount of CIP adsorbed onto the magnetic hybrid particles was determined using Eq. (1). The percentage of removal ($R$, %) was obtained from Eq. (2):

$$R = \frac{C_0 - C_t}{C_0} \times 100. \tag{2}$$

### Equilibrium adsorption studies

The equilibrium adsorption studies involved shaking solutions with different concentrations of CIP (from 40 to 1100 mg/L) with a fixed sorbent dose (0.5 mg/L) of the sorbent material for 24 h. The equilibrium adsorption experiments were conducted at pH = 5 and 25.0 ± 2.0 °C. The CIP adsorbed concentration at equilibrium was determined as defined by Eq. (1), but respectively replacing $q_t$ (mg/g) and $C_t$ (mg/L) by $q_e$ (mg/g) and $C_e$ (mg/g), where $C_e$ is the concentration of CIP at equilibrium.

### Regeneration and reuse of the magnetic hybrid particles

To further investigate the regeneration and reusability of the $Fe_3O_4$@$SiO_2$/κ-CRG/GPTMS, $Fe_3O_4$@$SiO_2$/ι-CRG/GPTMS and $Fe_3O_4$@$SiO_2$/λ-CRG/GPTMS particles, a fixed sorbent dosage (0.5 mg/mL) was tested in all the recycling cycles. The regeneration of the magnetic hybrid particles was evaluated after one adsorption cycle with CIP solution at a concentration of 100 mg/L for 24 h, at pH = 5. After that, CIP-loaded magnetic hybrid particles were magnetically collected from the solution and the regeneration process was conducted washing the particles with 10 mL KCl 1 M (four times), 10 mL distilled water (twice) and 10 mL ethanol (one time). Then, the magnetic hybrid particles were dried at 30 ℃ prior to reuse. The feasibility of the above-described regeneration method was evaluated using the regenerated magnetic hybrid particles in four consecutive adsorption/desorption cycles.

### Application in the removal of ciprofloxacin in wastewater samples

The wastewater sample used in this work was gathered at a local Aveiro's sewage treatment plants, after secondary treatment, corresponding to the final effluent. After collection, the wastewater sample was vacuum filtered through a 0.45 µm filter paper, to remove suspended residues. The pH and conductivity results were measured and are shown in Table S1, Supporting Information. The wastewater sample was spiked with CIP at an initial concentration of 5 mg/L and the pH was adjusting to 5. Selected sorbent doses of the magnetic hybrid particles (0.5, 1, 2.5 and 5 mg/mL) were added to the spiked CIP solution, and the mixtures were shaken for 24 h. Then, the magnetic hybrid particles were magnetically separated from the solution, and the remaining concentration of CIP in the treated water was analyzed by UV–VIS spectrophotometry at $\lambda_{max}$ 273 nm (Fig. S2, Supporting Information). The calibration curve was performed and used to convert the absorbance into CIP concentration in the wastewater samples (Fig. S2, Supporting Information).

## Results and discussion

### Materials characterization

The first step of this work consisted of synthesizing magnetite nanoparticles and their encapsulation in hybrid siliceous shells containing three types of carrageenans that vary in the degree of sulfation: κ-, ι-, and λ-carrageenan. The powder XRD patterns of the inorganic core showed the six characteristic X-ray diffraction peaks for $Fe_3O_4$ ($2\theta = 18.5°$, 30.1°, 35.5°, 43.3°, 53.6°, 57.1°, and 62.7°) ascribed to the reflections (1 1 1), (2 2 0), (3 1 1), (4 0 0), (4 2 2), (5 1 1), and (4 4 0), thus matching the reported diffraction pattern of magnetite (JCPDS file No. 19–0629) and confirming this iron oxide as the main crystalline phase present in the powdered samples (Fig. S3, Supporting Information). The $Fe_3O_4$ particles were then encapsulated through a one-step procedure by using either κ-, ι-, or λ-carrageenan/$SiO_2$ shells. This method involved the hydrolysis and condensation of a mixture of the silica precursor (tetraethyl orthosilicate, TEOS) and one of the modified polymers (κ-CRG/GPTMS, ι-CRG/GPTMS and λ-CRG/GPTMS), in the presence of the magnetic nanoparticles. The coated particles were magnetic and could be quickly attracted using a NdFeB bench magnet. Our previous studies have shown that spheroidal $Fe_3O_4$ nanoparticles of identical size are ferrimagnetic with small hysteresis loops and saturation magnetization of 83 emu.$g^{-1}$ [39]. A decrease in saturation magnetization is expected with the encapsulation owing to the mass contribution of the siliceous shell. Yet, this type of coating does not degrade the magnetic properties of the $Fe_3O_4$ core [39, 58]. Furthermore, coated particles still exhibited magnetic properties sufficiently high to achieve magnetic separation (Fig. S4, Supporting Information).

Further insight into the structure and composition of the hybrid shells was obtained from the analysis of non-magnetic hybrid particles obtained by the hydrolysis and condensation of TEOS with the modified polymers. The morphological characteristics of the magnetic hybrid particles and the non-magnetic hybrid particles were assessed by TEM and SEM, as depicted in Fig. 1 and Fig. S5 (Supporting Information), respectively. The TEM image of bare $Fe_3O_4$ particles shows nanoparticles with spherical shape and an average size of 56 ± 11 nm (Fig. 1a). TEM images of $Fe_3O_4$ coated particles show spheroidal nanoparticles uniformly coated by a shell. The shell thickness was about 18 ± 2 nm for $Fe_3O_4$@$SiO_2$/κ-CRG/GPTMS (Fig. 1b), 16 ± 2 nm for $Fe_3O_4$@$SiO_2$/ι-CRG/GPTMS (Fig. 1c) and 16 ± 5 nm for $Fe_3O_4$@$SiO_2$/ι-CRG/GPTMS (Fig. 1d) particles. Note that a similar thickness was observed for the bio-hybrid shell regardless of the biopolymer used. Conversely, the SEM analysis of the non-magnetic hybrid particles revealed a

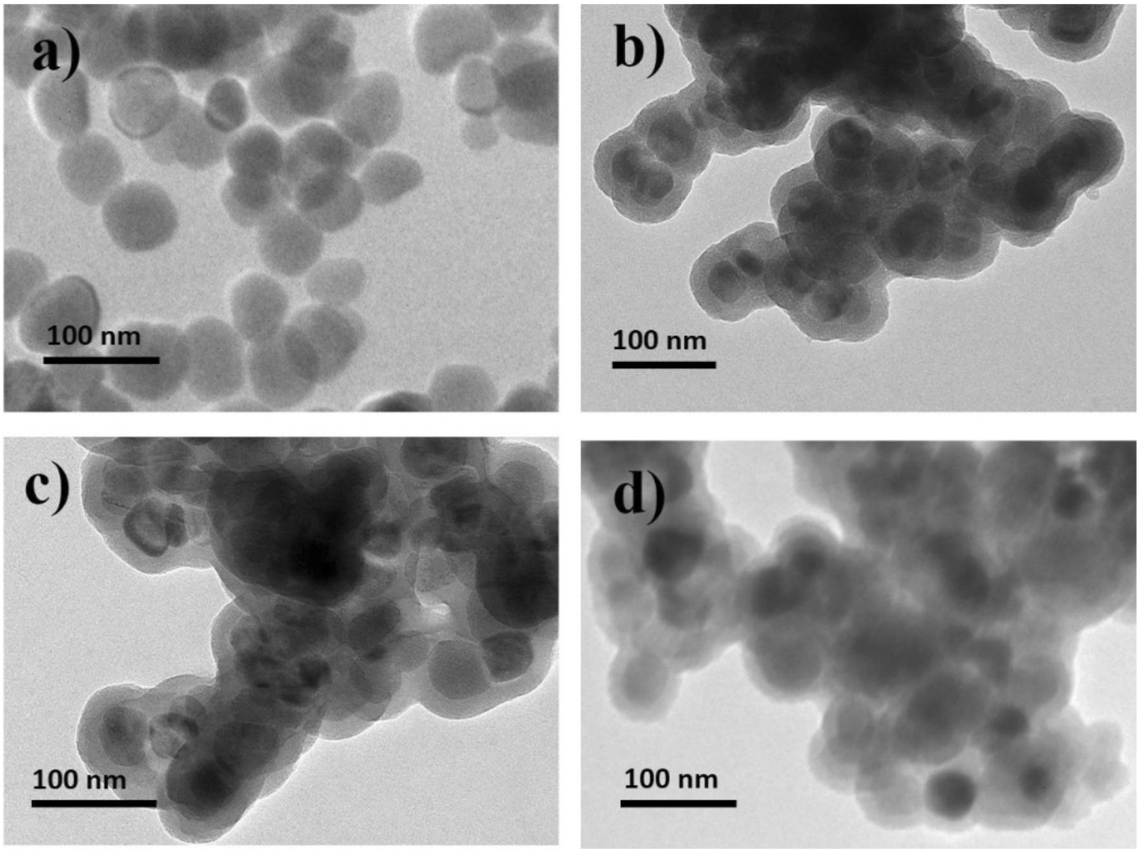


**Fig. 1** TEM images of the produced magnetic nanoparticles: **a** bare $Fe_3O_4$, **b** $Fe_3O_4$@$SiO_2$/κ-CRG/GPTMS, **c** $Fe_3O_4$@$SiO_2$/ι-CRG/GPTMS and **d** $Fe_3O_4$@$SiO_2$/λ-CRG/GPTMS

**Table 1** Compositional and structural properties of carrageenan-based materials: elemental analysis, particle diameter, BET surface area and pore volume

| Sample | C (%)[a] | H (%)[a] | N (%)[a] | S (%)[a] | D (nm)[b] | | $S_{BET}$ ($m^2$/g)[c] | $V_p$ ($cm^3$/g)[c] |
|---|---|---|---|---|---|---|---|---|
| | | | | | Core | Shell | | |
| $Fe_3O_4$ | 0.2 | 0.06 | 0.04 | – | 56 ± 11 | – | 27.4 | 0.066 |
| $Fe_3O_4$@$SiO_2$/κ-CRG/GPTMS | 23.2 | 3.70 | 0.27 | 3.3 | 56 ± 11 | 18 ± 2 | 6.1 | 0.006 |
| $Fe_3O_4$@$SiO_2$/ι-CRG/GPTMS | 13.0 | 2.10 | 0.20 | 3.2 | 56 ± 11 | 16 ± 2 | 6.3 | 0.005 |
| $Fe_3O_4$@$SiO_2$/λ-CRG/GPTMS | 15.5 | 2.60 | 0.30 | 3.9 | 56 ± 11 | 16 ± 5 | 9.0 | 0.015 |
| $SiO_2$/κ-CRG/GPTMS | 21.3 | 3.40 | 0.90 | 2.9 | 187 ± 15 | – | 4.6 | 0.006 |
| $SiO_2$/ι-CRG/GPTMS | 11.7 | 2.30 | 0.06 | 2.1 | 670 ± 250 | – | 3.4 | 0.002 |
| $SiO_2$/λ-CRG/GPTMS | 13.2 | 2.10 | 0.17 | 2.5 | 1101 ± 101 | – | 2.3 | 0.003 |

[a]C, H, N and S content assessed by elemental microanalysis

[b]Particle diameter measured by SEM

[c]BET surface area ($S_{BET}$) and pore volume ($V_p$) assessed by $N_2$ sorption.

well-defined spheroidal morphology but with markedly different average particle sizes depending on the type of carrageenan (Fig. S5, Supporting Information). Indeed, the average size was 187 ± 15 nm, 670 ± 250 nm and 1101 ± 101 nm for the non-magnetic hybrid particles prepared with κ-, ι-, and λ-carrageenan, respectively (Table 1). The results suggest that the average particle size increases with the degree of sulfation of the carrageenan.

The surface characteristics (specific surface area and pore volume) of the materials were determined by $N_2$ adsorption/desorption isotherms (Table 1). The BET surface area decreased from 27.4 $m^2$/g in $Fe_3O_4$ to 6.1, 6.3 and 9.0 $m^2$/g

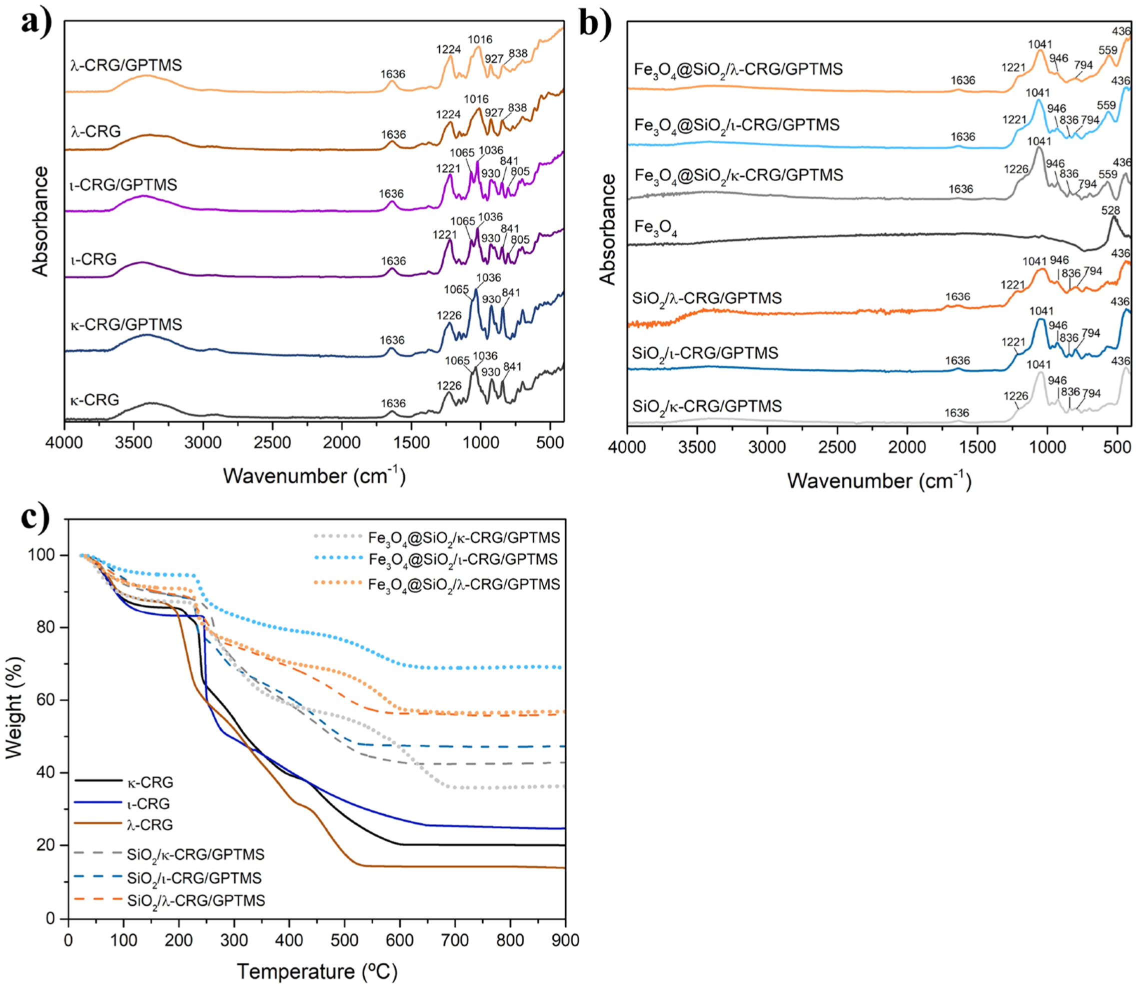


**Fig. 2** **a**, **b** ATR-FTIR spectra of carrageenan materials as indicated; **c** Thermograms of carrageenan based materials, performed under nitrogen atmosphere at a heating rate of 20 ºC/min

in $Fe_3O_4$@$SiO_2$/κ-CRG/GPTMS, $Fe_3O_4$@$SiO_2$/ι-CRG/GPTMS and $Fe_3O_4$@$SiO_2$/λ-CRG/GPTMS particles, respectively. The formation of the hybrid shell led to an increase of particle size and consequent decrease of the surface area. The pore volume is low, indicating that overall these are non-porous materials. Elemental microanalysis of the magnetic and non-magnetic hybrid particles (Table 1) shows a considerable amount of carbon content (12–23 wt %) due to the incorporation of the carrageenans and the presence of sulfur which originates in the ester sulfate groups of carrageenan. Although the carrageenans differ in the sulfate content in the following order κ- < ι- < λ-, the produced κ-carrageenan-based materials showed the highest sulfur content. This result indicates that the method is more efficient in incorporating κ-carrageenan in the hybrid materials, which is also confirmed by the higher carbon content present in the κ-carrageenan-based materials.

The FTIR spectra of κ-, ι-, and λ-carrageenan and the carrageenan-derivative Si alkoxides, κ-CRG/GPTMS, ι-CRG/GPTMS and λ-CRG/GPTMS (Fig. 2a), showed several bands in the anomeric region characteristic of the type of carrageenan and the degree of sulfation [59]. Briefly, κ-carrageenan showed absorption bands in the region 1065–1036 $cm^{-1}$ due to C–O and C–OH vibrations, a band at 841 $cm^{-1}$ ascribed to the α(1–3)-D-galactose C–O–S stretching vibration, a relatively strong band at approximately 930 $cm^{-1}$ indicating the presence of 3,6-anhydro-D-galactose and a broad band at 1226 $cm^{-1}$ that corresponds to the S–O asymmetric stretching of the ester sulfate groups (Fig. 2a) [60]. The FTIR spectrum of ι-carrageenan also shows the bands at approximately 930 $cm^{-1}$ and 841 $cm^{-1}$, with the same intensity pattern as in κ-carrageenan. However, an additional well-defined feature is visible in the spectrum, around 805 $cm^{-1}$, indicating the presence of sulfate ester in the 2-position of the anhydro-D-galactose residues, a characteristic band of the ι-carrageenan [61]. The FTIR spectrum of λ-carrageenan contains variable amounts of 2-sulfate ester groups, and presents high sulfate content as indicated by the broad band at 838 $cm^{-1}$–820 $cm^{-1}$ [62]. Furthermore, a broad band between 3500 $cm^{-1}$ and 3000 $cm^{-1}$ could be observed in carrageenan spectra and was assigned to hydrogen bonded O–H stretching vibrations [59]. All these vibrational bands are typical of κ-, ι-, and λ-carrageenan and have also been observed in the FTIR spectra of κ-CRG/GPTMS, ι-CRG/GPTMS and λ-CRG/GPTMS.

The FTIR spectrum of bare magnetite shows a strong band centered at 528 $cm^{-1}$ ascribed to the stretching vibration of the Fe–O bond in $Fe_3O_4$ (Fig. 2b) [56]. This band is also observed in the FTIR spectra of the coated magnetic hybrid particles although shifted to higher wavenumbers. The FTIR spectra of the magnetic and non-magnetic hybrid particles (Fig. 2b) also display the vibrational bands expected for a material comprising the polysaccharide and a siliceous network, and thus confirm the organic–inorganic hybrid nature of the materials. According to previous studies, the strong band at 436 $cm^{-1}$ ($\delta$(O–Si–O)) is an evidence of the formation of a siliceous network in both magnetic and non-magnetic hybrid particles [45]. Despite overlapping with vibrational features of carrageenan, the bands ascribed to amorphous silica are observed at 1041 $cm^{-1}$ ($\upsilon_{as}$(Si–O–Si)), 946 $cm^{-1}$ ($\upsilon$(Si–OH)) and at 794 $cm^{-1}$ ($\upsilon_s$(Si–O–Si)) [63].

The TGA of κ-, ι-, and λ-carrageenan-based materials are shown in Fig. 2c. The magnetic and non-magnetic hybrid particles showed higher thermal stability than the pristine polysaccharides, which is expected due to the presence of the inorganic component. Figure 2c also shows a similar thermal profile for all polysaccharide-based particles, namely the occurrence of three main stages of weight loss. The first stage of weight loss occurred in the temperature range of 60–150 °C. This is due to the evaporation of adsorbed water molecules H-bonded to –OH groups of the galactose units along the polymer chain [64]. The weight losses at this stage for all pristine carrageenan, magnetic and non-magnetic hybrid particles were 11–13%, 5–11% and 7–8%, respectively. In the second stage, the pristine carrageenans, magnetic and non-magnetic hybrid particles achieved total weight losses of 20–50%, 30–43% and 13–23% at 180–270 °C, 220–430 °C, and 220–260 °C, respectively. This stage was due to the decomposition of carrageenan polysaccharide chains, ascribed to carbohydrate-backbone fragmentation and sulfur dioxide release [65]. This thermolysis stage started at a higher temperature for the magnetic and non-magnetic hybrids derived from κ- and λ-carrageenan, as compared to the corresponding biopolymer, and indicates enhanced thermal stability most likely owing to the polysiloxane network. Further decomposition occurred afterwards, in a third stage. In the magnetic hybrids the onset temperature of the third decomposition stage markedly increased (~ 50 ºC) in comparison to non-magnetic hybrids. This result confirms the complex thermal degradation mechanism for these polymers in silica and magnetic particles, as reported in previous studies [64, 66–69]. At 900 °C, the residue of κ-, ι-, and λ-carrageenan was 20, 25 and 18 wt.%, respectively. At the same temperature, the magnetic and non-magnetic particles show a higher residue mass, ca. 36–68 wt.% and 42–55 wt.%, respectively, more than in the corresponding polymer counterpart, which is an evidence of the presence of a magnetic and siliceous inorganic components in the hybrid particles. Moreover, at 900 °C the magnetic and non-magnetic κ-carrageenan particles showed a weight loss of 64% and 58%, respectively, indicating higher thermal decomposition than in the ι- (32% and 53%) and λ-carrageenan-based (44% and 44%) particles. This result is in agreement with a high carbon content detected by elemental microanalysis (Table 1) in the κ-carrageenan-based particles.

Solid-state NMR spectroscopy analysis of non-magnetic hybrid particles was used to investigate the structure of the magnetic hybrid shells. The non-magnetic hybrid particles were prepared in the absence of $Fe_3O_4$ nanoparticles but with similar chemical composition as the shells. Figure 3 displays the $^{13}C$ cross-polarization (CP)/magic-angle spinning (MAS) NMR spectra for κ-, ι-, and λ-carrageenan and for the $SiO_2$/κ-CRG/GPTMS, $SiO_2$/ι-CRG/GPTMS, $SiO_2$/λ-CRG/GPTMS particles; the corresponding chemical-shift assignments are listed in Table S2 (Supporting Information). The $^{13}C$ NMR spectra of the non-magnetic hybrid particles showed resonances characteristic of the polysaccharide and the coupling agent GPTMS. In the range 60–105 ppm of the spectra, it was difficult to assign the resonances, due to several different C–O environments. When compared to the polysaccharide, the spectra of the non-magnetic hybrid particles shows new signals between 22 and 37 ppm, that are ascribed to the $C_a$ and $C_b$ carbon atoms of the Si-bonded propyl chain linked to GPTMS, as reported in the literature [70, 71]. The broad resonances between $\delta = 60$ ppm and 105 ppm have been attributed to the carbon atoms of κ-, ι-, and λ-carrageenan ($C_1$–$C_6$ and $C_1$–$C_6$) [72, 73]. In Fig. 3, the schematic representation showing the C sites labeling is merely illustrative of the covalent linkage between the siliceous network and the polysaccharide carrageenan. Based on these results, we could not discern the preferable substitution sites in the carrageenan macromolecules. The chemical shifts of κ-, ι-, and λ-carrageenan are given in Table S2 (Supporting Information). It should be noted that these assignments are close to the literature values [72–74]. The influence of sulfate groups is illustrated by the $^{13}C$ NMR spectrum of ι-carrageenan (Fig. 3b), which, compared to κ-carrageenan (Fig. 3a), has one more sulfate on the $C_{2'}$ carbon [73] (Fig. S6, Supporting Information). Moreover, the ι-carrageenan spectrum contains a very characteristic signal at 74.5 ppm attributed to $C_4$. This signal is absent in the spectra of other red algae polysaccharides [73], which is interpreted as the result of specific interaction between

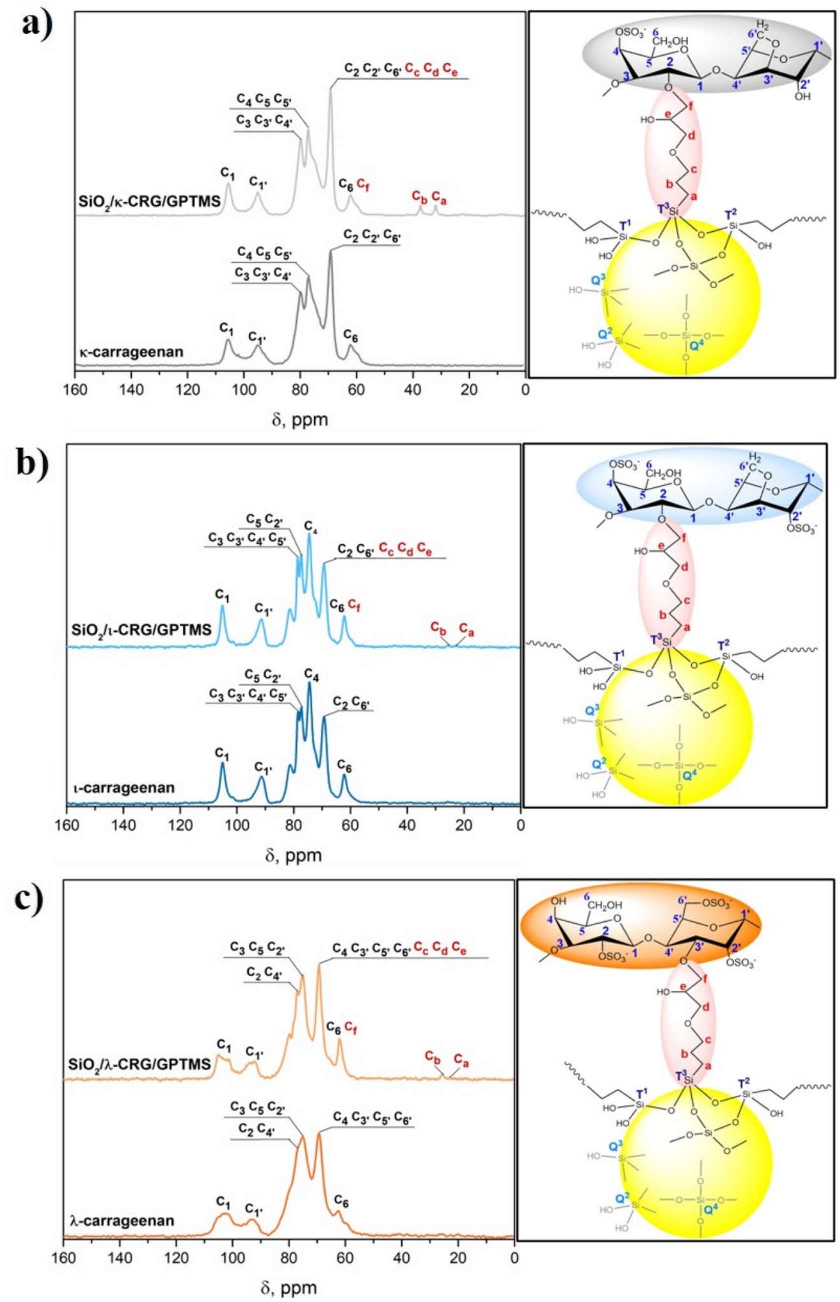


**Fig. 3** $^{13}C$ CP/MAS NMR spectra (left) and schematic representation (right) showing the labeling of C and Si sites according to NMR spectroscopy notation of **a** $SiO_2$/κ-CRG/GPTMS, **b** $SiO_2$/ι-CRG/GPTMS and **c** $SiO_2$/λ-CRG/GPTMS particles

two sulfate groups belonging to adjacent mono-saccharide residues in the ι-carrageenan [73]. The resulting $^{13}C$ NMR spectrum of λ-carrageenan (Fig. 3c) is composed of very broad signals, rather than clearly defined signals [72, 73]. Several anomeric carbons observed in the range of 103 ppm-93 ppm, demonstrate the absence of a single repeating unit in λ-carrageenan. The spectrum of λ-carrageenan showed anomeric signals at 102.5/101.9 attributed to $C_1$ of β-galactose 2-sulfate linked to α-anhydrogalactose [72–74] and $C_1$ of ß-galactose 2-sulfate linked to α-3,6 anhydrogalactose [74], as illustrated in Fig. S6, Supporting Information.

Solid-state $^{29}Si$ NMR spectroscopy was used to clarify the structure of the non-magnetic hybrid particles. The $^{29}Si$ MAS NMR and $^{29}Si$ CP/MAS NMR spectra of $SiO_2$/κ-CRG/GPTMS, $SiO_2$/ι-CRG/GPTMS and $SiO_2$/λ-CRG/GPTMS particles are shown in Fig. 4 (a and b, respectively). For comparison, the NMR spectra of amorphous $SiO_2$ particles prepared using the same methodology [57, 65] but in the absence of κ-CRG/GPTMS, ι-CRG/GPTMS and λ-CRG/GPTMS were also included in Fig. 4. The silicon sites are labeled in Fig. 3 according to the usual NMR spectroscopy notation: $Q^n$ is used to describe silica species where the silicon is bonded by $n$ bridging oxygens and $4-n$ non-bridging

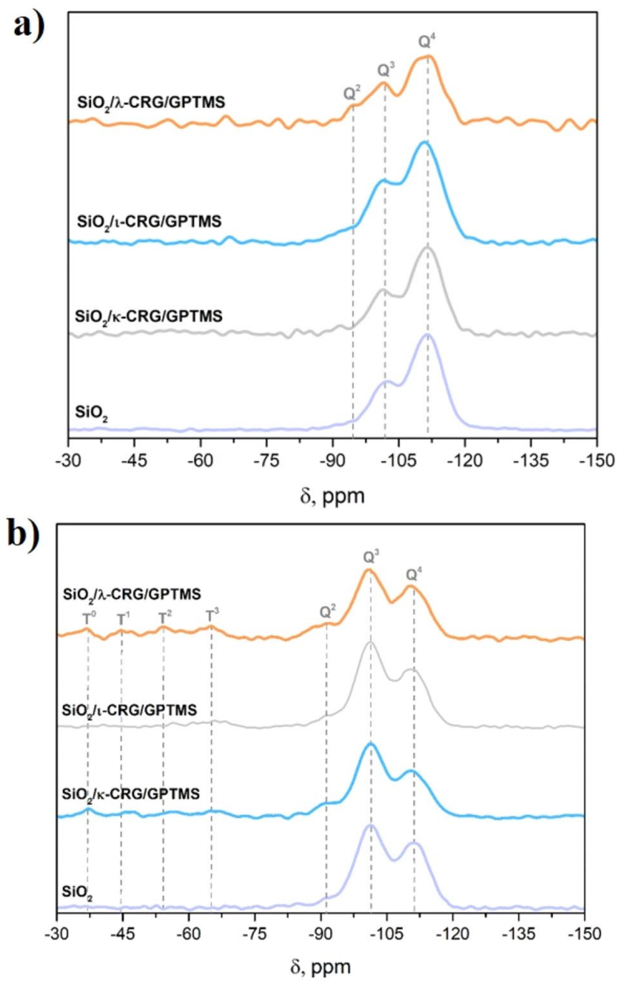


**Fig. 4** **a** $^{29}Si$ MAS NMR spectra and **b** $^{29}Si$ CP/MAS NMR spectra of $SiO_2$, $SiO_2$/κ-CRG/GPTMS, $SiO_2$/ι-CRG/GPTMS and $SiO_2$/λ-CRG/GPTMS particles

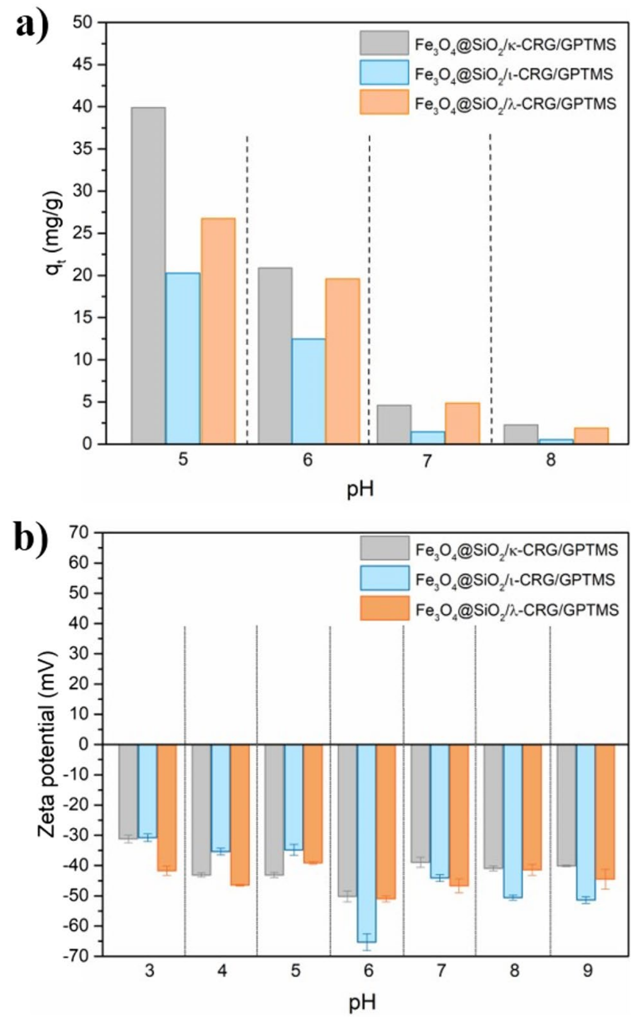


**Fig. 5** **a** Adsorption capacity of the hybrid sorbents as a function of pH (initial CIP concentration of 60 mg/L, 24-h contact time); **b** zeta potential values of magnetic colloidal particles

oxygens; $T^n$ represents a silicon atom bonded to carbon with $n$ bridging oxygens with $3-n$ non-bridging oxygens [65, 75, 76]. According to the literature, the resonances at $\delta = -94, -102$ and $-111$ ppm are normally assigned to $Q^2$, $Q^3$ and $Q^4$ sites, respectively (Fig. 4a) [56, 76]. From $^{29}Si$ MAS NMR spectra was calculated the fraction of silanol groups $((Q^2+Q^3)/Q^4)$ and was 0.52 in the $SiO_2$ particles, decreasing to 0.49, 0.37 and 0.50 in the $SiO_2$/κ-CRG/GPTMS, $SiO_2$/ι-CRG/GPTMS and $SiO_2$/λ-CRG/GPTMS particles, respectively (Table S3, Supporting Information). The decrease in the number of surface hydroxyl groups provides evidence for the covalent bonding of κ-CRG/GPTMS, ι-CRG/GPTMS and λ-CRG/GPTMS on the surface of the siliceous hybrid particles. Furthermore, the $^{29}Si$ CP/MAS NMR spectra of non-magnetic hybrid particles (Fig. 4b) show four resonances at approximately $\delta = -37.2$ ppm, –44.6 ppm, –54.3 ppm, and –65.3 ppm, which, compared to literature values, can be ascribed to the Si sites in $T^0$, $T^1$, $T^2$, and $T^3$, confirming the covalent bonding of carrageenan macromolecules to the siliceous network. The presence of $T^0$ species indicates that the hydrolysis of the three alkoxy groups of the κ-CRG/GPTMS, ι-CRG/GPTMS and λ-CRG/GPTMS can occur during the sol–gel reaction. These signals were more pronounced in the spectrum of $SiO_2$/λ-CRG/GPTMS than $SiO_2$/κ-CRG/GPTMS and $SiO_2$/ι-CRG/GPTMS particles.

## Removal of CIP using the magnetic hybrid particles

### Effect of pH

The effect of the pH on the ability of magnetic carrageenan-based hybrid particles to adsorb ciprofloxacin was examined at pH values ranging between 5 and 8. The presence of a carboxylic acid group ($pKa_1 = 5.9$) and a secondary amine group ($pKa_2 = 8.3$) in the ciprofloxacin molecule gives amphoteric behavior [77]. At pH < 5.9, CIP exists in the form of cationic species, while at the neutral pH it exists as a zwitterion, and the anionic form is the dominant species at higher pH. From the results in Fig. 5a, it was noticed that the adsorption capacity of CIP using the magnetic hybrid particles gradually decreased as the pH increased from 5 to 8.

The removal percentage of CIP also decreased when the pH increased from 5 to 8 (Fig. S7, Supporting Information). As shown in Fig. 5b, the colloidal particles present negatively charged surfaces between pH = 3 and 9; the observed high negative zeta potential values are explained by the presence of ionized ester sulfate groups of κ-, ι- and λ-carrageenan at the surface of the particles [78]. Hence, the adsorption at pH = 5 can be ascribed mainly to the electrostatic attraction between cationic ciprofloxacin species with protonated amine groups and the negative surface charge of $Fe_3O_4$@$SiO_2$/κ-CRG/GPTMS (-43.1 mV), $Fe_3O_4$@$SiO_2$/ι-CRG/GPTMS (– 34.8 mV) and $Fe_3O_4$@$SiO_2$/λ-CRG/GPTMS (– 39.1 mV) particles. This means that an increase in pH causes the fraction of cationic CIP species to decrease, and therefore the adsorption capacity decreases. At pH = 6, the fraction of cationic CIP should be considerable, close to 50% ($pKa_1 = 5.9$). However, at this pH, the adsorption capacity did not follow the trend of the zeta potential, with ι-carrageenan-based sorbents showing less adsorption capacity despite a more negative surface charge. This suggests that the sorption mechanism may involve other pathways, namely the hydrogen bonding formation between the CIP molecules and hydroxyl groups of the carrageenan [12]. Interestingly, the adsorption capacity of the materials followed the trend κ-CRG > λ-CRG > ι-CRG, regardless the pH investigated.

### Effect of contact time and initial CIP concentration

Figure 6 shows the time profile of the CIP uptake using the magnetic carrageenan-based hybrid particles for two initial concentrations of CIP (100 and 200 mg/L) during 180 min, at pH = 5, calculated from UV–VIS spectroscopy data (Fig. S8, Supporting Information). Regardless of the initial CIP concentration, the particles showed fast adsorption, reaching the maximum CIP adsorption after 60 min. Afterwards, the CIP adsorption slightly decreased and stabilized after 180 min (3 h) of contact time. The amount of CIP removed by the particles increased with the increase in CIP concentration (Fig. 6), suggesting that the CIP adsorption capacity by the particles was not exhausted in the CIP concentration tested. The removal percentage of CIP using $Fe_3O_4$@$SiO_2$/κ-CRG/GPTMS (50%) and $Fe_3O_4$@$SiO_2$/ι-CRG/GPTMS (20%) particles remained the same regardless of the initial CIP. However, the removal percentage of CIP using λ-CRG-based particles decreased steadily as CIP concentration increased (35% for 100 mg/L of CIP and 20%

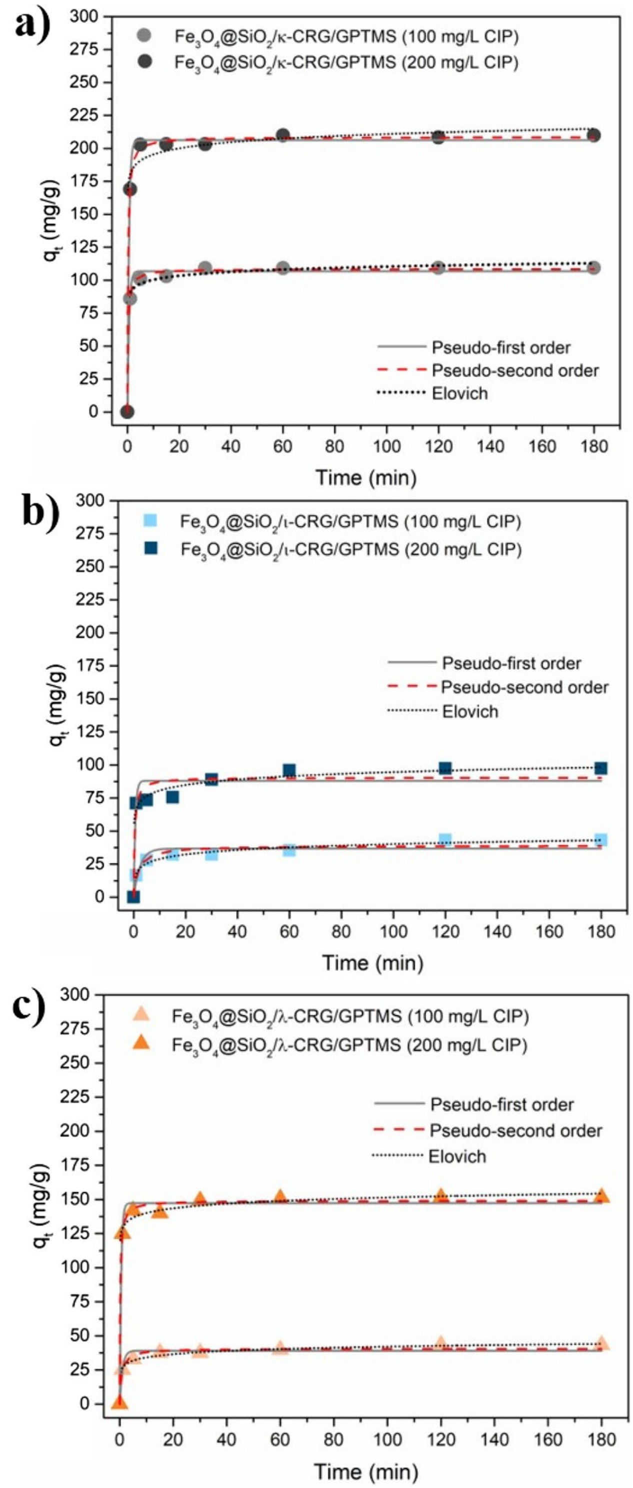


**Fig. 6** Time profile of adsorption capacity (initial CIP concentration of 100 and 200 mg/L, at pH = 5 for 180 min/3 h) using the particles **a** $Fe_3O_4$@$SiO_2$/κ-CRG/GPTMS, **b** $Fe_3O_4$@$SiO_2$/ι-CRG/GPTMS and **c** $Fe_3O_4$@$SiO_2$/λ-CRG/GPTMS, and the corresponding kinetic model fitting

for 200 mg/L of CIP) (Fig. S9, Supporting Information). These results suggest that the application of the particles for CIP removal might be most efficient at low concentrations (< 30 mg/L), which are most typical of natural aquatic environments where dilution is prevalent [79].

### Kinetic studies

The kinetics of CIP adsorption onto the three types of magnetic hybrid particles were fitted by pseudo-first-order [80], pseudo-second-order [81] and Elovich [82] models (Equations S1, S2 and S3, Supporting Information). The fitting curves are shown in Fig. 6 and the kinetic parameters of each model and the evaluation of the adequacy of the model fitting are reported in Tables S4, S5 and S6, Supporting Information. Two parameters (coefficient of determination ($R^2$) and Chi-square test value ($\chi^2$)) were used to evaluate the goodness of fits (Eqs. S4 and S5, Supporting Information). The $R^2$ and agreement between the experimental data ($q_e$, exp) and the calculated values ($q_e$, cal) indicate that the adsorption of CIP best follows a pseudo-second order kinetic model for $Fe_3O_4@SiO_2$/κ-CRG/GPTMS particles and Elovich model for $Fe_3O_4@SiO_2$/ι-CRG/GPTMS and $Fe_3O_4@SiO_2$/λ-CRG/GPTMS particles. The pseudo-second-order adsorption kinetics indicates strong interaction between CIP and adsorbent and is in agreement with other adsorption studies regarding pharmaceuticals [83, 84]. The Elovich model has been mostly employed to describe chemical sorption and considers that the solid surface is energetically heterogeneous [85]. The parameter α describes the initial adsorption rate, while β is an indicator of desorption. As shown in Tables S4, S5 and S6 (Supporting Information), the low values of β indicate effective interactions between CIP and the sorbents. Higher α values indicate faster initial CIP adsorption in $Fe_3O_4@SiO_2$/κ-CRG/GPTMS particles. Moreover, under the conditions tested, the removal efficiency was higher using κ-carrageenan-based particles (Fig. S9, Supporting Information).

### Equilibrium isotherms

The equilibrium adsorption isotherms of CIP by magnetic hybrid particles were studied by fitting the following models to data: Langmuir [86] and Freundlich [87] isotherms, which are two-parameter isotherms (Eqs. S6 and S7, Supporting Information, respectively), Sips isotherm [87], which is a three-parameter isotherm (Eq. S8, Supporting Information, respectively), and Dubinin–Radushkevich isotherm [88], that has been successfully used to describe sigmoidal isotherms (Eq. S9, Supporting Information). The simulated curves and all the isotherms parameters are summarized in Fig. 7 and Tables S7, S8 and S9, Supporting Information. Figure 7 showed that the equilibrium adsorption capacity

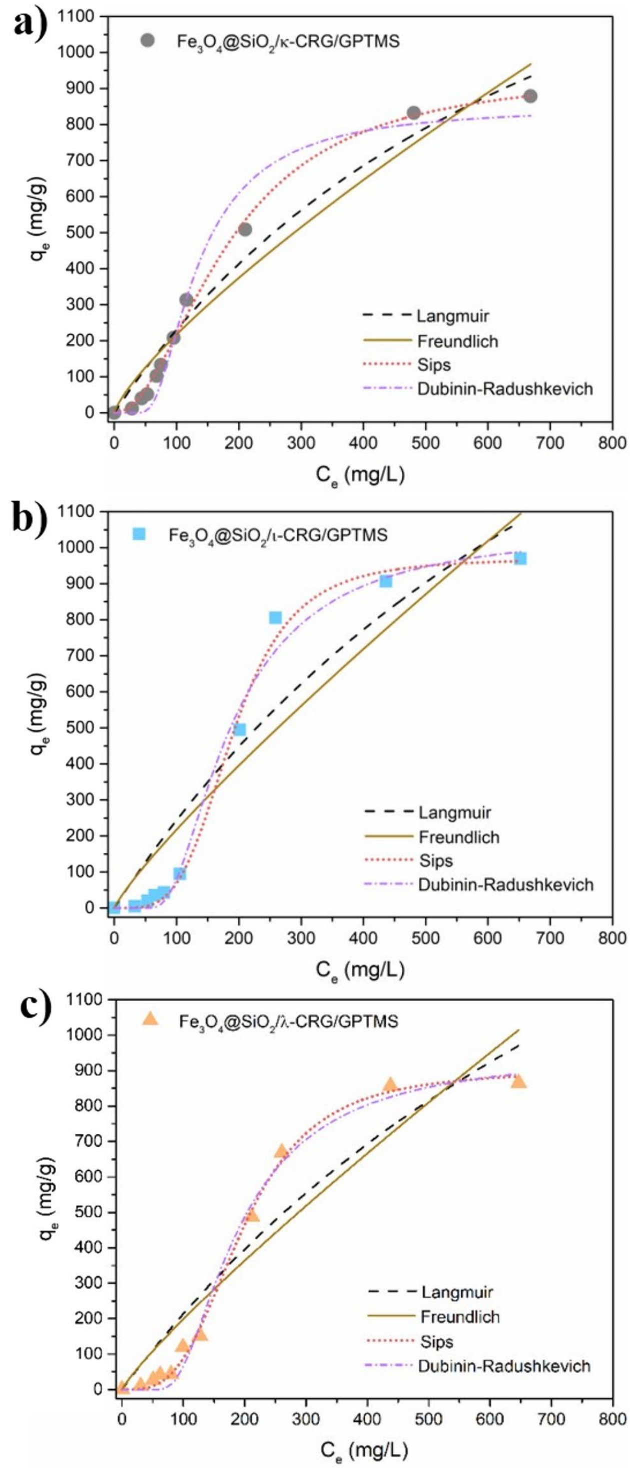


**Fig. 7** Isotherm data for the equilibrium adsorption of ciprofloxacin (CIP) on the **a** $Fe_3O_4@SiO_2$/κ-CRG/GPTMS, **b** $Fe_3O_4@SiO_2$/ι-CRG/GPTMS and **c** $Fe_3O_4@SiO_2$/λ-CRG/GPTMS particles, and model fitting

($q_e$) of magnetic particles increased with CIP's initial concentration. Considering the fitting indicators, the two-parameter isotherm that better describes the data for all systems is the Langmuir isotherm. However, the coefficient of determination ($R^2$) values obtained for the Langmuir adsorption isotherm model were relatively low, ranging from 0.965 to 0.889, indicating poor data fitting. Furthermore, the Langmuir model failed in predicting the maximum adsorption capacity ($q_{max}$) of the sorbent. The experimental $q_{max}$ value of κ-, ι- and λ-carrageenan based particles was 878.3, 969.3 and 865.1 mg/g, respectively, while the Langmuir model predicted values higher than 2000 mg/g. Thus, the Langmuir isotherm model significantly overestimated the maximum adsorption capacity of the particles, and for this reason, it was not appropriate to predict the experimental values. The maximum adsorption capacities of the produced κ-, ι- and λ-carrageenan-based materials were in the same order of magnitude, which could be explained by the similar sulfur content in the final materials.

The adsorption capacity for CIP was higher than many other sorbents [12], which suggested that the magnetic hybrid particles synthesized in this study had a broad spectrum of adsorption performance for CIP. Furthermore, it was observed that the adsorption capacity for CIP duplicates using the magnetic κ-carrageenan hybrid particles produced in this work, in comparison with a recent study reported by us with κ-carrageenan modified with a different coupling agent [39]. From the analysis of the fittings, the Sips and Dubinin–Radushkevich isotherms models adequately described the experimental data ($R^2 > 0.990$). The Sips isotherm is a combined form of the Langmuir and Freundlich isotherm models [87], while Dubinin–Radushkevich isotherm is applied to deduce the heterogeneity of the apparent adsorption energy on the adsorption site [88]. As the mean free energy expresses the energy for taking out a molecule from its adsorption site to the infinite, the Dubinin–Radushkevich isotherm model has been used for evaluation of nature of sorption, whether it is physical or chemical, between metal ions and pesticides [89–91]. The mean free energy, $E$ (kJ/mol) per mol of adsorbate, can be determined using Eq. (3), where $K_{DR}$ is the Dubinin–Radushkevich constant.

$$E = \frac{1}{\sqrt{2K_{DR}}}. \tag{3}$$

When the adsorption energy $E$ is less than 8 kJ/mol, it is indicative of physisorption (physical attachment of CIP molecule to the particles' surface); if $E$ is between 8 and 16 kJ/mol, the process is dominated by chemical ion-exchange mechanism and if the value of $E$ is greater than 16 kJ/mol reflects chemical interactions [39, 92]. The value of $E$ obtained in this work is 15.2, 10.9 and 10.7 kJ/mol for κ-, ι- and λ-carrageenan-based magnetic particles, respectively. These $E$ values for CIP adsorption on the sorbents indicate that the chemical ion-exchange mechanism is prevalent, similar to previous studies for CIP adsorption on other materials [39, 93]. These results suggest that in the adsorption process, protonated CIP molecules are exchanged with ester sulfate counterions in the polysaccharides κ-, ι- and λ-carrageenan.

The efficiency of the prepared particles for CIP removal was compared with other bio-based adsorbents reported in the literature. The maximum adsorption capacity was 878.3,

**Table 2** Comparison of the maximum CIP adsorption capacity ($q_{max}$) using several bio-based adsorbents reported in the literature

| Adsorbent | $q_{max}$ (mg/g) | Method of determination | References |
|---|---|---|---|
| $Fe_3O_4$@$SiO_2$/κ-CRG/GPTMS | 878.3 | Dubinin–Radushkevich | This work |
| $Fe_3O_4$@$SiO_2$/ι-CRG/GPTMS | 969.3 | Dubinin–Radushkevich | This work |
| $Fe_3O_4$@$SiO_2$/λ-CRG/GPTMS | 865.1 | Dubinin–Radushkevich | This work |
| Magnetic nanocomposites of alginate | 463.7 | Langmuir | [39] |
| Magnetic nanocomposites of κ-carrageenan | 426.6 | Langmuir | [39] |
| Magnetic nanocomposites of λ-carrageenan | 961.2 | Dubinin–Radushkevich | [39] |
| MgO/chitosan/graphene oxide nanosheets | 1111 | Langmuir | [94] |
| Activated carbon from bamboo | 613.0 | Experimental | [95] |
| Activated carbon from desilicated rice husk | 461.9 | Langmuir | [96] |
| Activated carbon from lignin | 418.6 | Langmuir | [97] |
| Al(III)-chelated cryogels of chitosan | 390.0 | Experimental | [98] |
| Modified alginate/graphene hydrogel | 344.8 | Langmuir | [99] |
| Sodium alginate/κ-carrageenan | 291.6 | Dubinin–Radushkevich | [100] |
| Magnetic chitosan/graphene oxide | 282.9 | Langmuir | [101] |
| $Fe_3O_4$/graphene oxide/biochar | 283.4 | Langmuir | [102] |
| Activated carbon from peach stones | 263.7 | Experimental | [103] |
| κ-Carrageenan/sodium alginate hydrogel | 229.0 | Experimental | [104] |
| Magnetite-imprinted chitosan | 142.9 | Langmuir | [105] |
| Sodium alginate/graphene oxide | 100.0 | Langmuir | [106] |

969.3 and 865.1 mg/g for the particles prepared using κ-, ι- and λ-carrageenan, respectively. As shown in Table 2, the developed particles effectively remove CIP and present maximum adsorption capacities higher than most reported bio-based adsorbents. In addition, these particles offer the advantage of fast separation and recovery from water using low-energy magnetic separation.

## Adsorption thermodynamics

Thermodynamic studies on CIP adsorption by the nanosorbents were conducted with varying reaction temperature (298 K, 308 K, and 318 K). Details of the experimental setup and the calculation methodology are described in Supporting Information and Fig. S10 (Supporting Information). The calculated thermodynamic parameters are summarized in Table 3. The negative values of the enthalpy change ($\Delta H$) indicated that the CIP adsorption was an exothermic process. This means that energy is released in heat to the surroundings, and adsorption is favored at a lower temperature. Indeed increasing the temperature resulted in less CIP removal (Table S10, Supporting Information). The magnitude of $\Delta H$ was low (~22–72 kJ/mol), which is more typical of physical adsorption. The heat of chemisorption generally falls into a higher range of 80–200 kJ/mol [107, 108]. Thus, a mechanism involving strong chemisorption purely can be excluded, which is in accordance with what was inferred from the values of the mean free energy ($E$) calculated using the Dubinin–Radushkevich isotherm. There is a decrease in entropy ($\Delta S<0$), which is in agreement with is an associative mechanism. The entropy decreases because CIP molecules change from a disorderly state in the aqueous medium, to a more orderly condition when adsorbed at the surface of the sorbent particles [109]. At 298 K, the adsorption was spontaneous ($\Delta G<0$) for κ-carrageenan-based sorbents ($Fe_3O_4$@$SiO_2$/κ-CRG/GPTMS) and non-spontaneous for the other sorbent particles. A slight increase of the $\Delta G$ values with the temperature was observed, indicating that the rise in the temperature was unfavorable for the spontaneity of adsorption. Similar behavior was observed for CIP adsorption onto κ-carrageenan/alginate hydrogels, being spontaneous at 293 K and 298 K but non-spontaneous at 303 K [100]. Positive $\Delta G$ values have been reported for the

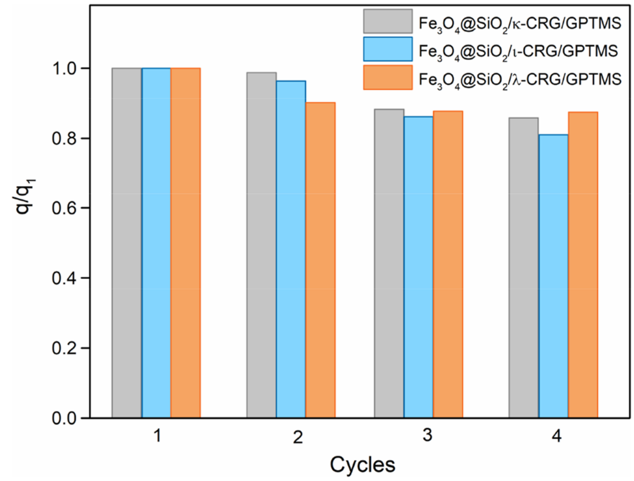


**Fig. 8** The ratio between the adsorption capacity ($q$) of ciprofloxacin (CIP) and the adsorption capacity after the first cycle ($q_1$) for $Fe_3O_4$@$SiO_2$/κ-CRG/GPTMS, $Fe_3O_4$@$SiO_2$/ι-CRG/GPTMS and $Fe_3O_4$@$SiO_2$/λ-CRG/GPTMS particles in four consecutive adsorption/desorption cycles (adsorption conditions: 100 mg/L CIP, pH = 5, contact time of 24 h)

adsorption of CIP onto coal fly ash and activated alumina [110] but, contrarily to this work, the process was endothermic and spontaneous at high temperature.

## Regeneration and reusability

From a practical point of view, the regeneration and reusability of the sorbents are essential features to consider for their technological application. Based on the mechanism analysis for the CIP adsorption process, the regeneration of the magnetic particles was performed by treatment using KCl 1 $mol.dm^{-3}$ [39, 45, 111]. Desorption of CIP after an adsorption experiment performed with the magnetic particles, was monitored by UV–VIS analysis of the aqueous solution used to rinse the particles (Fig. S11, Supporting Information). The CIP concentration in the supernatant decreased with the increasing number of rinsing steps, and no CIP was detected in the supernatant of the last rinsing, indicating that $K^+$ ions promoted the desorption of CIP from the magnetic hybrid particles. The adsorption–desorption cycles were repeated four times. As shown in Fig. 8, the recycled particles have

**Table 3** Thermodynamic parameters values for adsorption of ciprofloxacin using $Fe_3O_4$@$SiO_2$/κ-CRG/GPTMS, $Fe_3O_4$@$SiO_2$/ι-CRG/GPTMS and $Fe_3O_4$@$SiO_2$/λ-CRG/GPTMS particles

| Nanosorbent | Parameters | | | | |
|---|---|---|---|---|---|
| | $\Delta G$ (kJ/mol) | | | $\Delta S$ (J/mol K) | $\Delta H$ (kJ/mol) |
| | 298 K | 308 K | 318 K | | |
| $Fe_3O_4$@$SiO_2$/κ-CRG/GPTMS | – 1.87 | 0.47 | 2.81 | – 233.7 | – 71.5 |
| $Fe_3O_4$@$SiO_2$/ι-CRG/GPTMS | 1.04 | 2.51 | 3.98 | – 146.8 | – 42.7 |
| $Fe_3O_4$@$SiO_2$/λ-CRG/GPTMS | 1.37 | 2.15 | 2.93 | – 78.1 | – 21.9 |

maintained their ability toward CIP removal in all recycling steps. For all the particles, no significant differences were observed between the first and second adsorption cycles for the adsorption percentage (decreases < 10%). At the 4th cycle, the adsorption capacity of κ-, ι- and λ-carrageenan-based particles decreased nearly 15%, 19% and 13% relative to the initial adsorption capacity. The results further confirm that electrostatic interaction was the key driving force for CIP uptake. The regeneration experiments demonstrated that the as-designed magnetic hybrid particles possess good reusability.

### Removal of ciprofloxacin from wastewater samples

To preliminary assess the performance of the hybrid sorbents for CIP present in a more complex matrix, a wastewater sample was spiked with CIP (5 mg/L), and the pH was adjusted to 5. Figure 9 shows the percentage removal of CIP from ultra-pure water and wastewater samples. For all the magnetic hybrid particles, the percentage removal of CIP from wastewater was lower than in ultra-pure water. However, by increasing the sorbent dose from 0.5 to 5 mg/mL, the removal of CIP also increased in ultra-pure water and wastewater, indicating that the hybrid sorbents are still viable in these conditions. The decrease of CIP removal in real wastewater is expected, and it might be due to interference of natural organic matter and ions present in wastewater that competes with CIP for getting adsorbed. The reduction of the maximum absorbance of the real wastewater spiked with CIP over the treatment with the particles (Fig. S12, Supporting Information) confirmed the removal of CIP. Similar effects were observed when CIP was removed from river water using cellulose nanofibers and γ-$Al_2O_3$ nanoparticles [112, 113].

### Adsorption mechanism

Based on the results discussed above, the prevalent mechanism for CIP adsorption at pH = 5 onto these particles seems to be the ion-exchange between protonated CIP molecules and the counterions of the ester sulfate groups of the carrageenan polysaccharides. The $E$ values determined from the Dubinin–Radushkevich isotherm (from 10.7 to 15.2 kJ/mol) are in agreement with an ion-exchange mechanism. In addition, the low magnitude of $\Delta H$ values is in accordance with weak chemisorption processes such as ion exchange [107]. Because ion exchange is weak chemisorption, the process was reversible, and the sorbents particles could be regenerated through the treatment with aqueous KCl. An identical mechanism has been reported for CIP adsorption on other materials, such as clay minerals [114, 115] and magnetic resins [116].

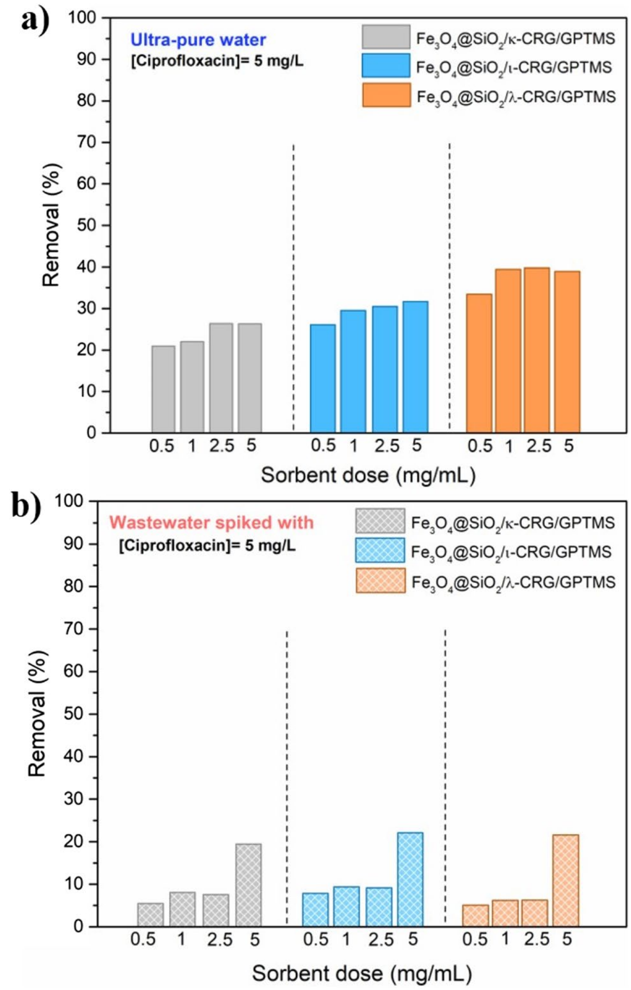


**Fig. 9** Removal efficiency of CIP from **a** ultra-pure water and **b** wastewater spiked with CIP (5 mg/L, at pH = 5 for 24 h) using several sorbent doses (0.5, 1, 2.5 and 5 mg/mL) of $Fe_3O_4$@$SiO_2$/κ-CRG/GPTMS, $Fe_3O_4$@$SiO_2$/ι-CRG/GPTMS and $Fe_3O_4$@$SiO_2$/λ-CRG/GPTMS particles

To investigate the nature of the interaction between the nanosorbents and CIP molecules, FTIR spectra of the nanosorbents after CIP adsorption (initial CIP concentration of 40 mg/L) were obtained and are depicted in Fig. S13, Supporting Information. The presence of CIP can be confirmed by the appearance of a well-defined band 1627 $cm^{-1}$, due to the ketone C=O stretching of CIP molecules. Further evidence of CIP adsorption is the appearance of the bands in the region of 1489 $cm^{-1}$ and 1459 $cm^{-1}$, which are ascribed to C–N stretching and protonation of amine group in piperazinyl moiety, respectively [117]. In the nanosorbents prepared from ι- and λ-carrageenan, these bands are less visible, which agrees with a lower CIP removal by these particles, for the initial CIP concentration tested. However, the disappearance of the C–O–S stretching band at ca. 840 $cm^{-1}$ of ι- and λ-carrageenan-based particles after CIP sorption is consistent with a sorption mechanism involving ester sulfate groups.

The sigmoidal shape of the adsorption isotherms indicated cooperative binding of CIP molecules [118]. Due to planar shape and hydrophobic character, CIP molecules have the propensity to self-aggregate and form clusters [119]. Thus, at lower CIP concentration, the CIP molecules interact mainly with the surface of the nanoparticles and adsorb via cation exchange mechanism, while as the CIP concentration increases, we might expect that CIP-CIP interaction will happen, leading to multilayer adsorption. Previously, it was found that the binding of the amphiphilic cationic drug doxazosin to carrageenans is cooperative in nature and that the strength of interactions increases with increasing negative charge of carrageenans [120]. The κ-, ι- and λ-carrageenan differ in the degree of sulfation and consequently on negative charge density. However, in our work, we could not find a clear correlation between CIP adsorption capacity of the sorbents and the carrageenan type. This may be because the sorbents particles here described presented similar sulfur content (Table 1) and no striking differences on the zeta potential values were observed, suggesting similar sulfation degree at the sorbents surface. Nevertheless, we could observe differences between the three sorbents, namely at the level of the sorption thermodynamics. Furthermore, at pH = 6 and above, the adsorption capacity of the three carrageenan sorbents was inconsistent with the zeta potential values. This indicates that other adsorption pathways, such as H-bond formation between CIP molecules and OH groups of carrageenan, may also co-exist [121, 122] besides electrostatic interaction and cation exchange (Fig. 10).

## Conclusions

In the present work, magnetic hybrid nanosorbents of κ-, ι- and λ-carrageenan were successfully prepared using a facile one-step method for the surface modification of magnetite nanoparticles. The synthetic strategy reported here seems to be more effective for incorporating κ-carrageenan in the hybrid siliceous shells. Although κ-carrageenan has a lower degree of sulfation, this biopolymer is cheaper than ι- and λ-carrageenan, advantageous in process costs. Furthermore, the produced magnetic hybrid particles using distinct carrageenans showed similar sulfur content. The resulting magnetic particles removed ciprofloxacin efficiently from ultra-pure water and wastewater samples. The maximum ciprofloxacin adsorption capacity of these magnetic sorbents in ultra-pure water (pH 5) was found to be > 865 mg/g in ultra-pure water, placing this material among one of the best magnetic systems for removing this pharmaceutical from water. CIP adsorption was described by a pseudo-second-order kinetic model for κ-carrageenan sorbents and Elovich model for the ι- and λ-carrageenan particles. The CIP adsorption onto the hybrid particles was a cooperative process, well described by the Dubinin–Radushkevich (DR) isotherm. The adsorption was exothermic ($\Delta H < 0$) and entropically favorable ($\Delta S < 0$) for the three types of particles. However, at 298 K, the adsorption was spontaneous ($\Delta G < 0$) for κ-carrageenan-based sorbents ($Fe_3O_4$@$SiO_2$/κ-CRG/GPTMS) and non-spontaneous for the other sorbent particles. The low magnitude of the enthalpy change ($-21.9 \leq \Delta H \leq -71.5$ kJ/mol) and low values of mean free

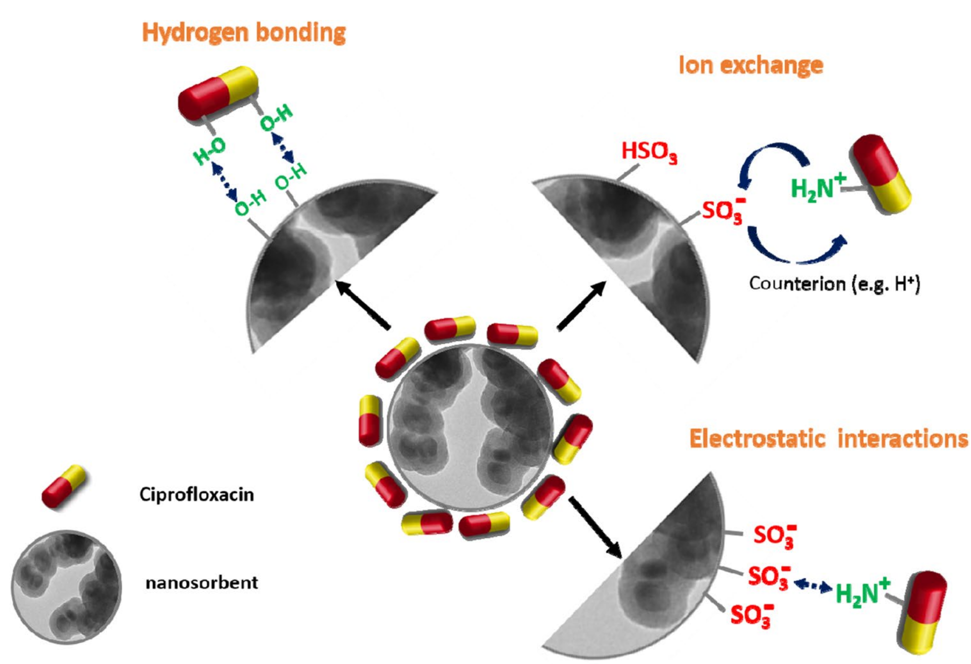


**Fig. 10** Scheme of plausible interactions between magnetic hybrid nanosorbents and CIP molecules

energy calculated from the DR isotherm ($10.7 \leq E \leq 15.2$ kJ/mol) pointed to ion exchange as the main mechanism for CIP removal by the magnetic hybrids. The improved efficiency obtained is related to the high affinity of ester sulfate groups from carrageenan polysaccharides, used here as surface modifiers, to cationic CIP molecules, along with reduced nanoparticle dimensions and high surface-to-volume ratio. The magnetic sorbents exhibited a good recycling performance up to 4 cycles, providing evidence for the cost-effectiveness of the method. The removal efficiency of CIP from wastewater was lower than in ultra-pure water. However, the results also show that by increasing the sorbent dosage, the removal efficiency also increases for both systems (ultra-pure water and wastewater), suggesting that after several sequential adsorption treatments, it is possible to achieve a significant removal of CIP from real water. Overall, the results obtained here allow us to anticipate that the proposed sorbents have an excellent potential for removing ciprofloxacin in environmental water samples.

**Supplementary Information** The online version contains supplementary material available at https://doi.org/10.1007/s40097-022-00498-x.

**Acknowledgements** This work was developed within the scope of the project CICECO-Aveiro Institute of Materials, UIDB/50011/2020, UIDP/50011/2020 & LA/P/0006/2020, financed by national funds through the FCT/MEC (PIDDAC). The authors thank the RNME (National Electronic Microscopy Network) for microscopy facilities. S. F. Soares thanks the Fundação para a Ciência e Tecnologia (FCT) for the PhD Grant SFRH/BD/121366/2016. J. Nogueira thanks the Fundação para a Ciência e Tecnologia (FCT) for the PhD Grant SFRH/BD/146249/2019. A. L. D.-d.-S. acknowledges FCT for the research contract under the Program' Investigador FCT' 2014 and for funding from the project IF/00405/2014.

## Declarations

**Conflict of interest** The authors declare no conflict of interest.

## References


1. Sabri, N.A., van Holst, S., Schmitt, H., et al.: Fate of antibiotics and antibiotic resistance genes during conventional and additional treatment technologies in wastewater treatment plants. Sci. Total Environ. **741**, 140199 (2020)
2. Tavengwa, N.T., Moyo, B., Musarurwa, H., et al.: Challenges and future directions in the analysis of emerging pollutants in aqueous environments. In: Dalu, T., Tavengwa, N.T. (eds.) Emerging Freshwater Pollutants, pp. 373–379. Elsevier (2022)
3. Sanganyado, E., Kajau, T.A.: The fate of emerging pollutants in aquatic systems: an overview. In: Dalu, T., Tavengwa, N.T. (eds.) Emerging Freshwater Pollutants, pp. 119–135. Elsevier (2022)
4. Burke, V., Richter, D., Greskowiak, J., et al.: Occurrence of antibiotics in surface and groundwater of a drinking water catchment area in germany. Water Environ. Res. **88**, 652–659 (2016)
5. Boy-Roura, M., Mas-Pla, J., Petrovic, M., et al.: Towards the understanding of antibiotic occurrence and transport in groundwater: findings from the Baix Fluvià alluvial aquifer (NE Catalonia, Spain). Sci. Total Environ. **612**, 1387–1406 (2018)
6. Gu, D., Feng, Q., Guo, C., et al.: Occurrence and risk assessment of antibiotics in manure, soil, wastewater, groundwater from livestock and poultry farms in Xuzhou, China. Bull. Environ. Contam. Toxicol. **103**, 590–596 (2019)
7. Van Doorslaer, X., Dewulf, J., Van Langenhove, H., Demeestere, K.: Fluoroquinolone antibiotics: an emerging class of environmental micropollutants. Sci. Total Environ. **500**, 250–269 (2014)
8. Rasheed, T., Bilal, M., Nabeel, F., et al.: Environmentally-related contaminants of high concern: potential sources and analytical modalities for detection, quantification, and treatment. Environ. Int. **122**, 52–66 (2019)
9. Sivagami, K., Vignesh, V.J., Srinivasan, R., et al.: Antibiotic usage, residues and resistance genes from food animals to human and environment: an Indian scenario. J. Environ. Chem. Eng. **8**, 102221 (2020)
10. Ahmadzadeh, S., Asadipour, A., Pournamdari, M., et al.: Removal of ciprofloxacin from hospital wastewater using electrocoagulation technique by aluminum electrode: optimization and modelling through response surface methodology. Process Saf. Environ. Prot. **109**, 538–547 (2017)
11. El-Shafey, E.-S.I., Al-Lawati, H., Al-Sumri, A.S.: Ciprofloxacin adsorption from aqueous solution onto chemically prepared carbon from date palm leaflets. J. Environ. Sci. **24**, 1579–1586 (2012)
12. Igwegbe, C.A., Oba, S.N., Aniagor, C.O., et al.: Adsorption of ciprofloxacin from water: a comprehensive review. J. Ind. Eng. Chem. **93**, 57–77 (2021)
13. Zhang, X., Tang, Y., Zhang, F., Lee, C.-S.: A novel aluminum-graphite dual-ion battery. Adv. Energy Mater. **6**, 1502588 (2016)
14. Wang, M., Jiang, C., Zhang, S., et al.: Reversible calcium alloying enables a practical room-temperature rechargeable calcium-ion battery with a high discharge voltage. Nat. Chem. **10**, 667–672 (2018)
15. Mu, S., Liu, Q., Kidkhunthod, P., et al.: Molecular grafting towards high-fraction active nanodots implanted in N-doped carbon for sodium dual-ion batteries. Natl. Sci. Rev. **8**, 1–12 (2020)
16. Chen, X., Wang, D., Wang, T., et al.: Enhanced photoresponsivity of a GaAs nanowire metal-semiconductor-metal photodetector by adjusting the fermi level. ACS Appl. Mater. Interfaces. **11**, 33188–33193 (2019)
17. Li, H., Tang, J., Kang, Y., et al.: Optical properties of quasi-type-II structure in GaAs/GaAsSb/GaAs coaxial single quantum-well nanowires. Appl. Phys. Lett. **113**, 233104 (2018)
18. Tang, X., Wu, J., Wu, W., et al.: Competitive-type pressure-dependent immunosensor for highly sensitive detection of diacetoxyscirpenol in wheat via monoclonal antibody. Anal. Chem. **92**, 3563–3571 (2020)
19. Zhu, W., Deng, M., Chen, D., et al.: Dual-phase CsPbCl3–Cs4PbCl6 perovskite films for self-powered, visible-blind UV photodetectors with fast response. ACS Appl. Mater. Interfaces. **12**, 32961–32969 (2020)
20. Xu, P., Cao, J., Yin, C., et al.: Quantum chemical study on the adsorption of megazol drug on the pristine BC3 nanosheet. Supramol. Chem. **33**, 63–69 (2021)
21. Zhao, C., Xi, M., Huo, J., et al.: Electro-reduction of $N_2$ on nanostructured materials and the design strategies of advanced catalysts based on descriptors. Mater. Today Phys. **22**, 100609 (2022)
22. Girardi, C., Greve, J., Lamshöft, M., et al.: Biodegradation of ciprofloxacin in water and soil and its effects on the microbial communities. J. Hazard. Mater. **198**, 22–30 (2011)
23. Wei, X., Chen, J., Xie, Q., et al.: Distinct photolytic mechanisms and products for different dissociation species of ciprofloxacin. Environ. Sci. Technol. **47**, 4284–4290 (2013)

24. Couto, C.F., Santos, A.V., Amaral, M.C.S., et al.: Assessing potential of nanofiltration, reverse osmosis and membrane distillation drinking water treatment for pharmaceutically active compounds (PhACs) removal. J. Water Process Eng. **33**, 101029 (2020)
25. Mu, Y., Huang, C., Li, H., Chen, L., et al.: Electrochemical degradation of ciprofloxacin with a Sb-doped $SnO_2$ electrode: performance, influencing factors and degradation pathways. RSC Adv. **9**, 29796–29804 (2019)
26. Fallah, Z., Zare, E.N., Ghomi, M., et al.: Toxicity and remediation of pharmaceuticals and pesticides using metal oxides and carbon nanomaterials. Chemosphere **275**, 130055 (2021)
27. Biswal, B.K., Balasubramanian, R.: Adsorptive removal of sulfonamides, tetracyclines and quinolones from wastewater and water using carbon-based materials: Recent developments and future directions. J. Clean. Prod. **349**, 131421 (2022)
28. Ahmad, I., Siddiqui, W.A., Ahmad, T.: Synthesis and characterization of molecularly imprinted magnetite nanomaterials as a novel adsorbent for the removal of heavy metals from aqueous solution. J. Mater. Res. Technol. **8**, 4239–4252 (2019)
29. Soares, S.F., Fernandes, T., Trindade, T., Daniel-da-Silva, A.L.: Recent advances on magnetic biosorbents and their applications for water treatment. Environ. Chem. Lett. **18**, 151–164 (2020)
30. Zare, E.N., Mudhoo, A., Khan, M.A., et al.: Water decontamination using bio-based, chemically functionalized, doped, and ionic liquid-enhanced adsorbents: review. Environ. Chem. Lett. **19**, 3075–3114 (2021)
31. Theamwong, N., Intarabumrung, W., Sangon, S., et al.: Activated carbons from waste *Cassia bakeriana* seed pods as high-performance adsorbents for toxic anionic dye and ciprofloxacin antibiotic remediation. Bioresour. Technol. **341**, 125832 (2021)
32. Wang, X., Wang, Y., Zhao, C., et al.: Ciprofloxacin removal by ultrasound-enhanced carbon nanotubes/permanganate process: in situ generation of free reactive manganese species via electron transfer. Water Res. **202**, 117393 (2021)
33. Huang, X., Tian, J., Li, Y., et al.: Preparation of a three-dimensional porous graphene oxide–kaolinite–poly(vinyl alcohol) composite for efficient adsorption and removal of ciprofloxacin. Langmuir **36**, 10895–10904 (2020)
34. Hu, Y., Pan, C., Zheng, X., et al.: Removal of ciprofloxacin with aluminum-pillared kaolin sodium alginate beads (CA-Al-KABs): kinetics, isotherms, and BBD model. Water (Basel) **12**, 905 (2020)
35. Falyouna, O., Maamoun, I., Bensaida, K., et al.: Encapsulation of iron nanoparticles with magnesium hydroxide shell for remarkable removal of ciprofloxacin from contaminated water. J. Colloid Interface Sci. **605**, 813–827 (2022)
36. Laabd, M., Brahmi, Y., el Ibrahimi, B., et al.: A novel mesoporous Hydroxyapatite@Montmorillonite hybrid composite for high-performance removal of emerging Ciprofloxacin antibiotic from water: Integrated experimental and Monte Carlo computational assessment. J. Mol. Liq. **338**, 116705 (2021)
37. Yang, Y., Zhong, Z., Li, J., et al.: Efficient with low-cost removal and adsorption mechanisms of norfloxacin, ciprofloxacin and ofloxacin on modified thermal kaolin: experimental and theoretical studies. J. Hazard. Mater. **430**, 128500 (2022)
38. Jiang, W.-T., Chang, P.-H., Wang, Y.-S., et al.: Removal of ciprofloxacin from water by birnessite. J. Hazard. Mater. **250**, 362–369 (2013)
39. Soares, S.F., Rocha, M.J., Ferro, M., et al.: Magnetic nanosorbents with siliceous hybrid shells of alginic acid and carrageenan for removal of ciprofloxacin. Int. J. Biol. Macromol. **139**, 827–841 (2019)
40. Yaashikaa, P.R., Senthil Kumar, P., Karishma, S.: Review on biopolymers and composites—evolving material as adsorbents in removal of environmental pollutants. Environ. Res. **212**, 113114 (2022)
41. Dang, B.-T., Bui, X.-T., Tran, D.P.H., et al.: Current application of algae derivatives for bioplastic production: a review. Bioresour. Technol. **347**, 126698 (2022)
42. Guo, Z., Wei, Y., Zhang, Y., et al.: *Carrageenan oligosaccharides*: a comprehensive review of preparation, isolation, purification, structure, biological activities and applications. Algal Res. **61**, 102593 (2022)
43. Zia, K.M., Tabasum, S., Nasif, M., et al.: A review on synthesis, properties and applications of natural polymer based carrageenan blends and composites. Int. J. Biol. Macromol. **96**, 282–301 (2017)
44. Papageorgiou, M., Nanaki, S., Kyzas, G., et al.: Novel isocyanate-modified carrageenan polymer materials: preparation, characterization and application adsorbent materials of pharmaceuticals. Polymers (Basel). **9**, 595 (2017)
45. Soares, S.F., Simões, T.R., António, M., et al.: Hybrid nanoadsorbents for the magnetically assisted removal of metoprolol from water. Chem. Eng. J. **302**, 560–569 (2016)
46. Sharma, G., Khosla, A., Kumar, A., et al.: A comprehensive review on the removal of noxious pollutants using carrageenan based advanced adsorbents. Chemosphere **289**, 133100 (2022)
47. Mohd Yusop, H., Mohd Ismail, A.I.H., Wan Ismail, W.N.: Preparation and characterization of new sol–gel hybrid inulin–TEOS adsorbent. Polymers (Basel). **13**, 1295 (2021)
48. Benvenuti, J., Giraldi Fisch, A., Zimnoch Dos Santos, J.H., Gutterres, M.: Hybrid sol–gel silica adsorbent material based on grape stalk applied to cationic dye removal. Environ. Prog. Sustain. Energy. **39**, 1–10 (2020)
49. Samiey, B., Cheng, C.-H., Wu, J.: Organic-inorganic hybrid polymers as adsorbents for removal of heavy metal ions from solutions: a review. Materials. **7**, 673–726 (2014)
50. Soares, S.F., Fateixa, S., Trindade, T., Daniel-da-Silva, A.L.: A versatile synthetic route towards gelatin-silica hybrids and magnetic composite colloidal nanoparticles. Adv. Compos. Hybrid. Mater. (2021). https://doi.org/10.1007/s42114-021-00386-y
51. Huang, Y., Keller, A.A.: Magnetic nanoparticle adsorbents for emerging organic contaminants. ACS Sustain. Chem. Eng. **1**, 731–736 (2013)
52. Kharissova, O.V., Dias, H.V.R., Kharisov, B.I.: Magnetic adsorbents based on micro- and nano-structured materials. RSC Adv. **5**, 6695–6719 (2015)
53. Malek, N.N.A., Jawad, A.H., Ismail, K., et al.: Fly ash modified magnetic chitosan-polyvinyl alcohol blend for reactive orange 16 dye removal: adsorption parametric optimization. Int. J. Biol. Macromol. **189**, 464–476 (2021)
54. Reghioua, A., Barkat, D., Jawad, A.H., et al.: Parametric optimization by Box-Behnken design for synthesis of magnetic chitosan-benzil/ZnO/$Fe_3O_4$ nanocomposite and textile dye removal. J. Environ. Chem. Eng. **9**, 105166 (2021)
55. Soares, S.F., Fernandes, T., Sacramento, M., et al.: Magnetic quaternary chitosan hybrid nanoparticles for the efficient uptake of diclofenac from water. Carbohydr. Polym. **203**, 35–44 (2019)
56. Oliveira-Silva, R., Pinto da Costa, J., Vitorino, R., Daniel-da-Silva, A.L.: Magnetic chelating nanoprobes for enrichment and selective recovery of metalloproteases from human saliva. J. Mater. Chem. B. **3**, 238–249 (2015)
57. Stöber, W., Fink, A., Bohn, E.: Controlled growth of monodisperse silica spheres in the micron size range. J. Colloid Interface Sci. **26**, 62–69 (1968)
58. Soares, S.F., Amorim, C.O., Amaral, J.S., et al.: On the efficient removal, regeneration and reuse of quaternary chitosan magnetite nanosorbents for glyphosate herbicide in water. J. Environ. Chem. Eng. **9**, 105189 (2021)

59. Gómez-Ordóñez, E., Rupérez, P.: FTIR-ATR spectroscopy as a tool for polysaccharide identification in edible brown and red seaweeds. Food Hydrocoll. **25**, 1514–1520 (2011)
60. Prado-Fernández, J., Rodríguez-Vázquez, J.A., Tojo, E., Andrade, J.M.: Quantitation of κ-, ι- and λ-carrageenans by mid-infrared spectroscopy and PLS regression. Anal. Chim. Acta. **480**, 23–37 (2003)
61. Pereira, L., Amado, A.M., Critchley, A.T., et al.: Identification of selected seaweed polysaccharides (phycocolloids) by vibrational spectroscopy (FTIR-ATR and FT-Raman). Food Hydrocoll. **23**, 1903–1909 (2009)
62. Pereira, L., Gheda, S.F., Ribeiro-Claro, P.J.A.: Analysis by vibrational spectroscopy of seaweed polysaccharides with potential use in food, pharmaceutical, and cosmetic industries. Int. J. Carbohydr. Chem. **2013**, 1–7 (2013)
63. Soares, S.F., Fernandes, T., Trindade, T., Daniel-da-Silva, A.L.: Trimethyl chitosan/siloxane-hybrid coated $Fe_3O_4$ nanoparticles for the uptake of sulfamethoxazole from water. Molecules **24**, 1958 (2019)
64. Wang, N., Teng, H., Li, L., et al.: Synthesis of phosphated k-carrageenan and its application for flame-retardant waterborne epoxy. Polymers (Basel). **10**, 1268 (2018)
65. Soares, S.F., Trindade, T., Daniel-da-Silva, A.L.: Carrageenan-silica hybrid nanoparticles prepared by a non-emulsion method. Eur. J. Inorg. Chem. **2015**, 4588–4594 (2015)
66. Ouyang, Z.-W., Chen, E.-C., Wu, T.-M.: Thermal stability and magnetic properties of polyvinylidene fluoride/magnetite nanocomposites. Materials **8**, 4553–4564 (2015)
67. Mahdavinia, G.R., Massoudi, A., Baghban, A., Shokri, E.: Study of adsorption of cationic dye on magnetic kappa-carrageenan/PVA nanocomposite hydrogels. J. Environ. Chem. Eng. **2**, 1578–1587 (2014)
68. Long, J., Wu, Z., Li, X., et al.: New method for the immobilization of pullulanase onto hybrid magnetic ($Fe_3O_4$–κ-carrageenan) nanoparticles by electrostatic coupling with pullulanase/chitosan complex. J. Agric. Food Chem. **63**, 3534–3542 (2015)
69. Kulal, P., Badalamoole, V.: Hybrid nanocomposite of kappa-carrageenan and magnetite as adsorbent material for water purification. Int. J. Biol. Macromol. **165**, 542–553 (2020)
70. Silva, R.R., Salvi, D.T.B., Santos, M.V., et al.: Multifunctional organic–inorganic hybrids based on cellulose acetate and 3-glycidoxypropyltrimethoxysilane. J. Sol-Gel Sci. Technol. **81**, 114–126 (2017)
71. Vueva, Y., Connell, L.S., Chayanun, S., et al.: Silica/alginate hybrid biomaterials and assessment of their covalent coupling. Appl. Mater. Today. **11**, 1–12 (2018)
72. van de Velde, F., Pereira, L., Rollema, H.S.: The revised NMR chemical shift data of carrageenans. Carbohydr. Res. **339**, 2309–2313 (2004)
73. Turquois, T., Acquistapace, S., Vera, F.A., Welti, D.H.: Composition of carrageenan blends inferred from $^{13}$C-NMR and infrared spectroscopic analysis. Carbohydr. Polym. **31**, 269–278 (1996)
74. Silva, F.R.F., Dore, C.M.P.G., Marques, C.T., et al.: Anticoagulant activity, paw edema and pleurisy induced carrageenan: action of major types of commercial carrageenans. Carbohydr. Polym. **79**, 26–33 (2010)
75. Babonneau, F., Baccile, N., Laurent, G., et al.: Solid-state nuclear magnetic resonance: A valuable tool to explore organic-inorganic interfaces in silica-based hybrid materials. C. R. Chim. **13**, 58–68 (2010)
76. Barberena-Fernández, A.M., Carmona-Quiroga, P.M., Blanco-Varela, M.T.: Interaction of TEOS with cementitious materials: Chemical and physical effects. Cem. Concr. Compos. **55**, 145–152 (2015)
77. Chen, L., Yuan, T., Ni, R., et al.: Multivariate optimization of ciprofloxacin removal by polyvinylpyrrolidone stabilized NZVI/Cu bimetallic particles. Chem. Eng. J. **365**, 183–192 (2019)
78. Schefer, L., Adamcik, J., Mezzenga, R.: Unravelling secondary structure changes on individual anionic polysaccharide chains by atomic force microscopy. Angew. Chem. Int. Ed. **53**, 5376–5379 (2014)
79. Khan, N.A., Najam, T., Shah, S.S.A., et al.: Development of Mn-PBA on GO sheets for adsorptive removal of ciprofloxacin from water: kinetics, isothermal, thermodynamic and mechanistic studies. Mater. Chem. Phys. **245**, 122737 (2020)
80. Lagergren, S.: Zur theorie der sogenannten adsorption gelöster stoffe. Springer-Verlag (1907)
81. Ho, Y.S., McKay, G.: Pseudo-second order model for sorption processes. Process Biochem. **34**, 451–465 (1999)
82. Chien, S.H., Clayton, W.R.: Application of Elovich equation to the kinetics of phosphate release and sorption in soils. Soil Sci. Soc. Am. J. **44**, 265 (1980)
83. Bui, T.X., Choi, H.: Adsorptive removal of selected pharmaceuticals by mesoporous silica SBA-15. J. Hazard. Mater. **168**, 602–608 (2009)
84. Sotelo, J.L., Rodríguez, A.R., Mateos, M.M., et al.: Adsorption of pharmaceutical compounds and an endocrine disruptor from aqueous solutions by carbon materials. J. Environ. Sci. Health Part B **47**, 640–652 (2012)
85. Wu, F.-C., Tseng, R.-L., Juang, R.-S.: Characteristics of Elovich equation used for the analysis of adsorption kinetics in dye-chitosan systems. Chem. Eng. J. **150**, 366–373 (2009)
86. Langmuir, I.: The adsorption of gases on plane surfaces of glass, mica and platinum. J. Am. Chem. Soc. **40**, 1361–1403 (1918)
87. Freundlich, H.Z.: Concerning adsorption in solutions. Z. Phys. Chem. **57**, 444–448 (1906)
88. Dubinin, M.M., Radushkevich, L.V.: Equation of the characteristic curve of activated charcoal. Proc. Acad. Sci. USSR Sect. C Phys. Chem. **55**, 331–333 (1947)
89. Togue Kamga, F.: Modeling adsorption mechanism of paraquat onto Ayous (*Triplochiton scleroxylon*) wood sawdust. Appl. Water Sci. **9**, 1 (2019)
90. Ayawei, N., Ebelegi, A.N., Wankasi, D.: Modelling and interpretation of adsorption isotherms. J. Chem. **2017**, 3039817 (2017)
91. Çelebi, O., Üzüm, Ç., Shahwan, T., Erten, H.N.: A radiotracer study of the adsorption behavior of aqueous Ba2+ ions on nanoparticles of zero-valent iron. J. Hazard. Mater. **148**, 761–767 (2007)
92. Mutavdžić Pavlović, D., Ćurković, L., Grčić, I., et al.: Isotherm, kinetic, and thermodynamic study of ciprofloxacin sorption on sediments. Environ. Sci. Pollut. Res. **24**, 10091–10106 (2017)
93. Awe, A.A., Opeolu, B.O., Fatoki, O.S., et al.: Preparation and characterisation of activated carbon from Vitisvinifera leaf litter and its adsorption performance for aqueous phenanthrene. Appl. Biol. Chem. **63**, 12 (2020)
94. Nazraz, M., Yamini, Y., Asiabi, H.: Chitosan-based sorbent for efficient removal and extraction of ciprofloxacin and norfloxacin from aqueous solutions. Mikrochim. Acta. **186**, 459 (2019)
95. Wang, Y.X., Ngo, H.H., Guo, W.S.: Preparation of a specific bamboo based activated carbon and its application for ciprofloxacin removal. Sci. Total Environ. **533**, 32–39 (2015)
96. Zhang, B., Han, X., Gu, P., et al.: Response surface methodology approach for optimization of ciprofloxacin adsorption using activated carbon derived from the residue of desilicated rice husk. J. Mol. Liq. **238**, 316–325 (2017)
97. Huang, L., Wang, M., Shi, C., et al.: Adsorption of tetracycline and ciprofloxacin on activated carbon prepared from lignin with $H_3PO_4$ activation. Desalin. Water Treat. **52**, 2678–2687 (2014)
98. Privar, Y., Shashura, D., Pestov, A., et al.: Metal-chelate sorbents based on carboxyalkylchitosans: Ciprofloxacin uptake by Cu(II) and Al(III)-chelated cryogels of N-(2-carboxyethyl)chitosan. Int. J. Biol. Macromol. **131**, 806–811 (2019)

99. Zhuang, Y., Yu, F., Ma, J., Chen, J.: Enhanced adsorption removal of antibiotics from aqueous solutions by modified alginate/graphene double network porous hydrogel. J. Colloid Interface Sci. **507**, 250–259 (2017)
100. Li, L., Zhao, J., Sun, Y., et al.: Ionically cross-linked sodium alginate/κ-carrageenan double-network gel beads with low-swelling, enhanced mechanical properties, and excellent adsorption performance. Chem. Eng. J. **372**, 1091–1103 (2019)
101. Wang, F., Yang, B., Wang, H., et al.: Removal of ciprofloxacin from aqueous solution by a magnetic chitosan grafted graphene oxide composite. J. Mol. Liq. **222**, 188–194 (2016)
102. Zhou, Y., Cao, S., Xi, C., et al.: A novel $Fe_3O_4$/graphene oxide/citrus peel-derived bio-char based nanocomposite with enhanced adsorption affinity and sensitivity of ciprofloxacin and sparfloxacin. Bioresour. Technol. **292**, 121951 (2019)
103. Álvarez-Torrellas, S., Peres, J.A., Gil-Álvarez, V., et al.: Effective adsorption of non-biodegradable pharmaceuticals from hospital wastewater with different carbon materials. Chem. Eng. J. **320**, 319–329 (2017)
104. Yu, F., Cui, T., Yang, C., et al.: κ-Carrageenan/Sodium alginate double-network hydrogel with enhanced mechanical properties, anti-swelling, and adsorption capacity. Chemosphere **237**, 124417 (2019)
105. Rasoulzadeh, H., Mohseni-Bandpei, A., Hosseini, M., Safari, M.: Mechanistic investigation of ciprofloxacin recovery by magnetite–imprinted chitosan nanocomposite: Isotherm, kinetic, thermodynamic and reusability studies. Int. J. Biol. Macromol. **133**, 712–721 (2019)
106. Zhao, P., Yu, F., Wang, R., et al.: Sodium alginate/graphene oxide hydrogel beads as permeable reactive barrier material for the remediation of ciprofloxacin-contaminated groundwater. Chemosphere **200**, 612–620 (2018)
107. Saha, P., Chowdhury, S.: Insight into adsorption thermodynamics. In: Tadashi, M. (ed.) Thermodynamics, pp. 349–364. InTech, Vienna (2011)
108. Husein, D.Z.: Adsorption and removal of mercury ions from aqueous solution using raw and chemically modified Egyptian mandarin peel. Desalin. Water Treat. **51**, 6761–6769 (2013)
109. Liu, S.: Cooperative adsorption on solid surfaces. J. Colloid Interface Sci. **450**, 224–238 (2015)
110. Maheshwari, M., Vyas, R.K., Sharma, M.: Kinetics, equilibrium and thermodynamics of ciprofloxacin hydrochloride removal by adsorption on coal fly ash and activated alumina. Desalin. Water Treat. **51**, 7241–7254 (2013)
111. Soares, S.F., Simões, T.R., Trindade, T., Daniel-da-Silva, A.L.: Highly efficient removal of dye from water using magnetic carrageenan/silica hybrid nano-adsorbents. Water Air Soil Poll. **228**, 87 (2017)
112. Nemati Sani, O., Navaei fezabady, A.A., Yazdani, M., Taghavi, M.: Catalytic ozonation of ciprofloxacin using $\gamma$-$Al_2O_3$ nanoparticles in synthetic and real wastewaters. J. Water Process Eng. **32**, 100894 (2019)
113. Das, S., Barui, A., Adak, A.: Montmorillonite impregnated electrospun cellulose acetate nanofiber sorptive membrane for ciprofloxacin removal from wastewater. J. Water Process Eng. **37**, 101497 (2020)
114. Wang, C.-J., Li, Z., Jiang, W.T., et al.: Cation exchange interaction between antibiotic ciprofloxacin and montmorillonite. J. Hazard. Mater. **183**, 309–314 (2010)
115. Wang, Y., Nie, Q., Huang, B., et al.: Removal of ciprofloxacin as an emerging pollutant: a novel application for bauxite residue reuse. J. Clean. Prod. **253**, 120049 (2020)
116. Wang, W., Cheng, J., Jin, J., et al.: Effect of humic acid on ciprofloxacin removal by magnetic multifunctional resins. Sci. Rep. **6**, 30331 (2016)
117. Ma, S., Si, Y., Wang, F., et al.: Interaction processes of ciprofloxacin with graphene oxide and reduced graphene oxide in the presence of montmorillonite in simulated gastrointestinal fluids. Sci. Rep. **7**, 2588 (2017)
118. Inglezakis, V.J., Poulopoulos, S.G., Kazemian, H.: Insights into the S-shaped sorption isotherms and their dimensionless forms. Micropor. Mesopor. Mat. **272**, 166–176 (2018)
119. Li, J., Beuerman, R., Verma, C.: The effect of molecular shape on oligomerization of hydrophobic drugs: molecular simulations of ciprofloxacin and nutlin. J. Chem. Phys. **148**, 104902 (2018)
120. Pavli, M., Baumgartner, S., Kos, P., Kogej, K.: Doxazosin–carrageenan interactions: a novel approach for studying drug–polymer interactions and relation to controlled drug release. Int. J. Pharm. **421**, 110–119 (2011)
121. Liu, X., Lu, S., Liu, Y., et al.: Adsorption of sulfamethoxazole (SMZ) and ciprofloxacin (CIP) by humic acid (HA): characteristics and mechanism. RSC Adv. **7**, 50449–50458 (2017)
122. Zhang, H., Khanal, S.K., Jia, Y., et al.: Fundamental insights into ciprofloxacin adsorption by sulfate-reducing bacteria sludge: Mechanisms and thermodynamics. Chem. Eng. J. **378**, 122103 (2019)




## Authors and Affiliations

**Sofia F. Soares[1] · João Nogueira[1] · Tito Trindade[1] · Ana L. Daniel-da-Silva[1]**

✉ Ana L. Daniel-da-Silva
ana.luisa@ua.pt

[1] Department of Chemistry, CICECO-Aveiro Institute of Materials, University of Aveiro, 3810-193 Aveiro, Portugal